



Atmospherically-forced sea-level variability in western Hudson Bay, Canada

Igor A. Dmitrenko¹, Denis L. Volkov^{2,3}, Tricia A. Stadnyk⁴, Andrew Tefs⁴, David G. Babb¹, Sergei A. Kirillov¹, Alex Crawford¹, Kevin Sydor⁵, and David G. Barber¹

- 5 ¹Centre for Earth Observation Science, University of Manitoba, Winnipeg, Manitoba, Canada
²Cooperative Institute for Marine and Atmospheric Studies, University of Miami, Miami, Florida, USA
³NOAA, Atlantic Oceanographic and Meteorological Laboratory, Miami, Florida, USA
⁴Department of Geography, University of Calgary, Calgary, Alberta, Canada
⁵Manitoba Hydro, Winnipeg, Manitoba, Canada

10 *Correspondence to:* Igor A. Dmitrenko (igor.dmitrenko@umanitoba.ca)

Abstract. In recent years, significant trends toward earlier breakup and later freeze-up of sea-ice in Hudson Bay have led to a considerable increase in shipping activity through the Port of Churchill, which is located in western Hudson Bay and is the only deep-water ocean port in the province of Manitoba. Therefore, understanding sea level variability at the Port is an urgent issue crucial for safe navigation and coastal infrastructure. Using tidal gauge data from the Port along with an atmospheric reanalysis and Churchill River discharge, we assess environmental factors impacting synoptic to seasonal variability of sea-level at Churchill. An atmospheric vorticity index used to describe the wind forcing was found to correlate with sea level at Churchill. Statistical analyses show that, in contrast to earlier studies, local discharge from the Churchill River can only explain up to 5% of the sea level variability. The cyclonic wind forcing contributes from 22% during the ice-covered winter-spring season to 30% during the ice-free summer-fall season due to cyclone-induced storm surge generated along the coast. Multiple regression analysis revealed that wind forcing and local river discharge combined can explain up to 32% of the sea level variability at Churchill. Our analysis further revealed that the seasonal cycle of sea level at Churchill appears to be impacted by the seasonal cycle in atmospheric circulation rather than by the seasonal cycle in local discharge from the Churchill River, particularly post-construction of the Churchill River diversion in 1977. Sea level at Churchill shows positive anomalies for September-November compared to June-August. This seasonal difference was also revealed for the entire Hudson Bay coast using satellite-derived sea level altimetry. This anomaly was associated with enhanced cyclonic atmospheric circulation during fall, reaching a maximum in November, which forced storm surges along the coast. Complete sea-ice cover during winter impedes momentum transfer from wind stress to the water column, reducing the impact of wind forcing on sea level variability. Expanding our observations to the bay-wide scale, we confirmed the process of wind-driven sea-level variability with (i) tidal-gauge data from eastern Hudson Bay and (ii) satellite altimetry measurements. Ultimately, we find that cyclonic winds generate sea level rise along the western and eastern coasts of Hudson Bay at the synoptic and seasonal time scales, suggesting an amplification of the bay-wide cyclonic geostrophic circulation in fall (October-November), when cyclonic vorticity is enhanced, and Hudson Bay is ice-free.



1 Introduction

Hudson Bay in northeast Canada is a shallow (mean depth ~ 150 m), semi-enclosed sub-arctic inland sea that is connected to the Labrador Sea through Hudson Strait (Figure 1). The Bay occupies approximately 831,000 km², making it the world's largest inland sea, and is characterized by a high annual volume of river discharge (712 km³; Déry et al., 2005; 2011) and a dynamic seasonal ice cover that exists from November/December to June/July (Hochheim and Barber, 2010; 2014). Prevailing cyclonic winds drive cyclonic circulation of water within the Bay (e.g., Ingram and Prinsenber, 1998; Saucier et al., 2004; St-Laurent et al., 2011; Ridenour et al., 2019a; Dmitrenko et al., 2020). Model simulations by Saucier et al. (2004) show that the cyclonic circulation is stronger during fall, reaching a maximum in November when the winds are strongest, and weakest in spring when Hudson Bay has a complete sea-ice cover. Dmitrenko et al. (2020), however, found that even during the ice covered season strong cyclones can amplify cyclonic water circulation in the Bay. This is consistent with conclusions by St-Laurent et al. (2011), who noted that momentum is transmitted through the mobile ice pack to the water column. Both velocity measurements (Prinsenber, 1986b; Ingram and Prinsenber, 1998; Dmitrenko et al., 2020) and model simulations (Wang et al., 1994; Saucier et al., 2004; St-Laurent et al., 2011; Ridenour et al., 2019b) show that during summer, cyclonic water circulation produces a cyclonic coastal transport corridor that advects riverine water along the coast toward Hudson Strait and into the Labrador Sea.

The local water mass of Hudson Bay is dominated by freshwater input comprised of river runoff from the largest watershed in Canada and sea-ice meltwater (e.g., Prinsenber, 1984, 1988, 1991; Saucier and Dionne, 1998; Granskog et al., 2009; Eastwood et al., 2020). The annual mean discharge rate of $22.6 \times 10^3 \text{ m}^3 \text{ s}^{-1}$ corresponds to a net discharge of 712 km³ of freshwater per year (Déry et al., 2005, 2011). In April, about $742 \pm 10 \text{ km}^3$ of freshwater withdrawn from the surface water layer by ice growth (Landy et al., 2017). Freshwater transport in Hudson Bay exhibits a strong seasonal cycle influenced by the timing of river discharge (e.g., Déry et al., 2005), the annual melt/freeze cycle of sea ice (Ingram and Prinsenber, 1998; Saucier et al., 2004; Straneo and Saucier, 2008; Granskog et al., 2011), and seasonality of wind forcing (Saucier et al., 2004; St-Laurent et al., 2011).

During the last decade, significant progress has been achieved in understanding the Hudson Bay environmental system (e.g., Granskog et al., 2009; Kuzyk et al., 2011; St-Laurent et al., 2011; Piecuch and Ponte, 2015; Kuzyk and Candlish, 2019; Eastwood et al., 2020; Dmitrenko et al., 2020, 2021). However, the synoptic, seasonal, and interannual variability of sea level in Hudson Bay still remains insufficiently studied due to a scarcity of sea level observations at permanent tidal gauges. Note that the tidal gauge in Churchill (Figure 1) is the only continuously operating tide gauge in Hudson Bay and the central Canadian Arctic. Historically, the focus of sea level studies in Hudson Bay was motivated by this area's post-glacial isostatic rebound (e.g., Guttenberg, 1941; Tushingham, 1992); for a detailed review of these earlier studies see Wolf et al. (2006). The advent of space-geodesy, in particular GPS, absolute-gravimetry, and satellite altimetry measurements (e.g., Larson and van Dam, 2000; Wolf et al., 2006; Sella et al., 2007) afforded a shift in focus for Hudson Bay sea level research to environmental aspects related to global warming and hydroelectric regulation (Gough, 1998, 2000),



and those associated with increasing the shipping traffic from the Port of Churchill through Hudson Bay to Hudson Strait, which may soon become a federally-designated transportation corridor (e.g., Andrews et al., 2017; Pew Charitable Trusts, 2016).

In 2016, the University of Manitoba and Manitoba Hydro launched a project on “Variability and change of
70 freshwater-marine coupling in the Hudson Bay System”, named BaySys, which aimed to assess the relative contributions of climate change and river regulation to the Hudson Bay system. Here, we are specifically focused on the impact of the Churchill River diversion on variability of sea level at the Port of Churchill. Additionally, we put our findings in the context of wind forcing over the entire Hudson Bay, elaborating on the suggestion by Dmitrenko et al. (2020) that cyclonic wind forcing generates onshore Ekman transport and storm surges along the coast.

We also revisit earlier results by Gough and Robinson (2000) and Gough et al. (2005). Using tidal gauge and river
75 discharge data from 1974 to 1994, Gough and Robinson (2000) suggested that the Churchill River discharge dominates sea-level variability at Churchill. They explained the seasonal elevation of sea level during late fall by a recirculating mechanism that links the spring pulse of river discharge in the downstream James Bay (Figure 1) to sea level at Churchill (Gough and Robinson, 2000; Gough et al., 2005). In this paper, we present an alternative mechanism and show that (i) the Churchill
80 River discharge plays a secondary role for generating sea level anomalies at Churchill, and (ii) the synoptic and seasonal variability of sea level at Churchill and over the entire Hudson Bay is impacted by the wind forcing described with an atmospheric vorticity index (Figure 2).

2 Data

2.1 Sea level

The daily mean sea level data used in this study were retrieved from the Canadian Tides and Water Levels Data Archive of
85 the Fisheries and Oceans Canada through <http://www.isdm-gdsi.gc.ca/isdm-gdsi/twl-mne/index-eng.htm#s5>. Measurements of sea level at Churchill were obtained from the permanent tidal gauge that is installed at the port of Churchill (station #5010) near the mouth of the Churchill River (Figure 1). This is the only permanently operating tide gauge in Hudson Bay and the central Canadian Arctic. While measurements of sea level at Churchill date back to the 1930s (Gutenberg, 1941), we
90 only used data from 1950 to present (Figure 3a), which is coincident with atmospheric reanalysis data from the National Centers for Environmental Prediction (NCEP; Kalnay et al., 1996). In addition, we used sea level data from the temporary tidal gauge in Innujuak (station #4575), Cape Jones Island (station #4656), and North Kopak Island (station #4548) (Figure 1). Among these three locations, only data at Innujuak are fully representative for our analysis because they span a sufficiently long period from October 1969 to October 1980, however, only the portion of this time series from September
95 1973 to December 1975 is continuous. Sea level records at Cape Jones Island and North Kopak Island are from August-October 1973 and 1975, respectively, and were selected among other temporary stations in Hudson Bay to overlap with sea level time series at Innujuak.



Satellite altimetry data from 1993-2020 were used to analyze the relationship between wind forcing and sea level changes over the entire Hudson Bay. We used the daily fields of absolute dynamic topography (ADT), i.e. the sea surface height above geoid, processed and distributed by Copernicus Marine and Environment Monitoring Service (CMEMS; <https://marine.copernicus.eu/>). The ADT is obtained by adding a mean dynamic topography (DT2018, Mulet et al., 2013) to sea level anomaly (SLA) measured by altimetry satellites. The SLA/ADT fields are computed using data from all satellites available at a given time following a methodology described in Pujol et al. (2016). Prior to mapping, altimetry records are corrected for instrumental noise, orbit determination error, atmospheric refraction, sea state bias, static and dynamic atmospheric pressure effects, and tides. Because in this work we are interested in local (dynamic) changes of sea level, the global mean sea level was subtracted from each ADT map. Then the seasonal climatology was computed for July through August (JJA) and September through November (SON). Sea ice does not represent a significant problem for computing the climatology, because Hudson Bay is essentially ice free during these months, especially during SON.

2.2 River discharge

Churchill River discharge data were obtained from Déry et al. (2016) and extended to 2019; thus, we use a continuous record of daily mean discharge from 1960 to 2019 (Figure 4a). The record was constructed from gauged observations above Red Head Rapids (station #06FD001), which is located ~87 km from the Churchill River mouth and is the most downstream hydrometric gauge along the Churchill River. When these data were not available, we used upstream gauges (applying a drainage area correction) to fill significant gaps in the time series (see Déry et al. 2016 for detailed methods). Data were adjusted by drainage area (between the hydrometric gauge location and river outlet) and any significant tributary inflows were added to represent discharge at the outlet of the Churchill River.

2.3 Wind forcing

Fields of sea level pressure (SLP) and 10-m wind velocity at 6-h intervals were derived from the NCEP atmospheric reanalysis. We chose the NCEP reanalysis to extend the atmospheric forcing data back to 1950, which covers the tide gauge record from Churchill, while a previous comparison of wind speeds from NCEP and ERA5 (Copernicus Climate Change Service, 2017; Hersbach et al., 2020) with in situ observations from the Churchill weather station revealed an insignificant discrepancy between the two reanalyses and meteorological observations (Dmitrenko et al., 2020). Cyclones over the Hudson Bay area were manually tracked using the NCEP SLP fields, with the central position and low SLP tabulated. The horizontal resolution of the NCEP-derived data is 2.5° of latitude and longitude.

125 3 Methods

For the 1950/60–2019 study period, a vorticity index was derived from the daily mean SLP NCEP data to characterize the wind forcing and compare to the time series of sea level anomalies (Figures 2a, 3a, and 4a). The vorticity index gives both



the sign and magnitude of atmospheric vorticity; it was first proposed by Walsh et al. (1996) and then successfully used for describing atmospheric forcing over the Siberian shelves (Dmitrenko et al., 2008a; 2008b) and Hudson Bay (Dmitrenko et al., 2020). The vorticity index is defined as the numerator of the finite difference Laplacian of SLP for an area within a radius of 550 km centered at 60°N and 85°W in Hudson Bay (Figure 1). A positive index corresponds to cyclonic atmospheric circulation that is typically associated with northerly winds in western Hudson Bay, whereas a negative vorticity index corresponds to anticyclonic atmospheric circulation characterized by southerly winds in western Hudson Bay (Figure 2). Dmitrenko et al. (2020) examined the spatial uncertainty of atmospheric vorticity estimated at 60°N, 85°W by computing vorticity for the 5-point stencils with a central node shifted relative to 60°N, 85°W by approximately 280 km northward, eastward, southward, and westward. Their results show that vorticity computed at 60°N, 85°W best describes major cyclonic storms observed in 2016–2017.

The vorticity index used in this study does not fully explain the observed variability of meridional wind in western Hudson Bay (Figure 2b), which is mainly responsible for generating storm surge along the coast (Dmitrenko et al., 2020). However, vorticity describes the intensity of cyclonic wind forcing over the entire Bay impacting the basin-scale circulation and sea level deformations along the entire coastline of Hudson Bay (Dmitrenko et al., 2020). Thus, our approach allowed us to extend our findings over the entire Bay. We also conducted a validation comparing the NCEP-derived vorticity to that derived from the ERA5 SLP utilizing the Web-Based Reanalysis Intercomparison Tools described by Smith et al. (2014). The comparison showed insignificant differences between the two reanalyses: the NCEP-derived vorticity only slightly exceeds that obtained from ERA5, while the correlation between the NCEP and ERA5-derived vorticities is 0.96 (Figure 2a).

The Churchill River discharge time series (Figure 4a) was compiled as follows. First, no significant gaps in Churchill River discharge record occurred on a daily basis. There were, however, some missing discharge data between 1976 and 1995, with some gaps up to 3 months (e.g., 1984, 1987). When data gaps occurred, then the upstream hydrometric gauge below Fidler Lake (station #06FB001) was used to infill data, with streamflow data adjusted to account for the difference in contributing area between Fidler Lake and the Churchill outlet, following the procedure of Déry et al. (2005). When the upstream hydrometric data were also unavailable, a secondary step was taken to infill data gaps. Missing data on a given day were infilled using the day-of-year mean value of streamflow over the available period of record. This procedure constructed a daily climatology of streamflow (i.e., mean annual hydrograph) based on the availability of data over the period of record.

For the Churchill River, however, we constructed a separate climatology of daily streamflow for the periods prior to and after flow diversion in 1977. Partial diversion began in 1976, allowing less than the full capacity of discharge to be diverted into the Nelson River system, with full operation beginning in 1977. We therefore designated 1977 as the first year when diversion became operational.

It is also important to separate the pre- and post-regulation periods for the analysis of the potential impact natural (pre-diversion) and regulated Churchill River discharge have on sea level anomalies at Churchill. Déry et al. (2016) reported that the Churchill River diversion caused a significant decline in the mean annual discharge from $37.0 \pm 4.2 \text{ km}^3 \text{ year}^{-1}$ pre-diversion (1964–73) compared to post-diversion flows (8.4 ± 2.9 and $9.6 \pm 4.4 \text{ km}^3 \text{ year}^{-1}$ for 1984–93 and 1994–2003,



respectively). Déry et al. (2016) further revealed the coefficient of variation (*CV*) of annual Churchill River discharge increased in inter-decadal *CV* post-diversion (1984–2013; $CV = 0.35\text{--}0.67$) compared to pre-diversion records (1964–1973; $CV = 0.11$). Both the decline in mean annual discharge and increase in discharge variability for the post-diversion period necessitate separate analysis of the impact of river discharge on sea level variability due to non-stationarity in the discharge record, which was implemented in our analysis.

The sea level record in Churchill is impacted by the post-glacial isostatic adjustment, with present-day uplift in the Hudson Bay area of $\sim 10\text{ mm year}^{-1}$ (e.g., Sella et al., 2007). Combining satellite altimeter data with the Churchill tide-gauge data gives an uplift rate of about $9.0 \pm 0.8\text{ mm year}^{-1}$ (Ray, 2015). The crustal uplift is evident in the negative sea level trend at Churchill of about the same magnitude (Figure 3a). To examine synoptic to seasonal variability of sea level at Churchill, a polynomial fit was subtracted from the data (Figure 3a). Thus, in our study we examined the sea level anomalies (SLA) against the low-frequency trend conditioned by the post-glacial isostatic adjustment. In addition, the daily mean tide gauge data were corrected for inverted barometer effect using sea-level atmospheric pressure from the NCEP reanalysis.

We used multiple linear regression to estimate a partial contribution of the cyclonic wind forcing and Churchill River discharge to SLA. In this context, multiple regression uses the least squares method to calculate the value of SLA based on the two independent variables as the vorticity index and Churchill River discharge.

4 Results

In this section, we examine the impact of cyclonic wind forcing and local river discharge on sea level variability at Churchill. We analyze (4.1) SLA at Churchill, (4.2) atmospheric vorticity over Hudson Bay, (4.3) the Churchill River discharge, and (4.4) their correlations.

4.1 Sea level

The 30-day running mean of SLA at Churchill ranging from 0.39 m in October 1973 to -0.36 m in April 1981 is dominated by the seasonal cycle (Figure 4a, blue line). In terms of the long-term monthly mean, sea level shows a seasonal cycle with positive anomalies $> 0.09\text{ m}$ from September–November and negative anomalies of about -0.14 m from March–April (Figure 5a).

There is a substantial difference in the seasonal patterns of sea level between the pre- and post-diversion periods. The long-term variability of sea level (Figure 3a) and SLA (Figure 4a) shows no abrupt disruption with the introduction of the Churchill River diversion in 1977. However, the seasonal cycle of SLA generated for pre- and post-diversion shows a characteristic difference in the timing and magnitude of SLA (Figure 5a). First, for the natural seasonal cycle prior to 1977 (blue line in Figure 5a), SLA shows two seasonal peaks in June ($\sim 0.04\text{ m}$; standard error of the mean $\sigma = \pm 0.01\text{ cm}$) and November ($\sim 0.11\text{ m}$, $\sigma = \pm 0.02\text{ cm}$). Post-diversion, SLA shows no peak in June, but the magnitude of positive anomalies in September and October increased to $> 0.08\text{ m}$. This result is consistent with findings by Gough and Robinson (2000). In



contrast to summer, during February-May, the pre- and post-diversion magnitude of SLA decreased and increased, respectively, by $\geq \pm 0.02$ m relative to the long-term monthly mean (Figure 5a). The standard deviation of the monthly mean values is up to 0.1 m (error bars in Figure 5a). The seasonal pattern of SLA was partially disrupted in 1981-82 and 1987-88, and significantly diminished in 1962-63 and 2016-17 (Figures 3a and 4a).

A closer look at the daily data reveals that the sea level seasonal maximum from October-November is modulated by storm surges frequently observed during the late fall. For example, in 1969-70 and 2003-04 (highlighted with yellow shading on Figure 4), the seasonal cycle of sea level (Figure 6, thick light blue line) was impacted by synoptic-scale events dominant during October-November (Figure 6, blue line). These storm surges lasted from ~ 3 to 6 days and correspond to positive anomalies of up to 0.5 m in the daily mean sea level (Figure 6b). In contrast, from December to May, the number and magnitude of storm surges gradually decrease (Figure 6).

205

4.2 Wind forcing

The vorticity index shows predominant cyclonic atmospheric circulation over Hudson Bay (mostly positive values in Figure 3a, red line), which agrees with results presented by *Saucier et al.* (2004) and *St-Laurent et al.* (2011). The strongest positive (cyclonic) vorticity is observed from fall 1962 to winter 1963 (vorticity index exceeded 14 s^{-1}), while the strongest negative (anticyclonic) atmospheric forcing (vorticity $< 4 \text{ s}^{-1}$) is recorded during summer 1963 (Figure 3a). Overall, the alternation between monthly mean cyclonic and anticyclonic wind forcing is mostly governed by the seasonal cycle in vorticity (Figure 5b). The monthly mean cyclonic vorticity increases from 4 s^{-1} in September to $\sim 8 \text{ s}^{-1}$ in November, and then gradually returns to $\sim 4 \text{ s}^{-1}$ in February (Figure 5b). During March-May and August, cyclonic vorticity is relatively low ($< 2 \text{ s}^{-1}$), and only in June and July does vorticity change to weak anticyclonic (slightly negative) values (Figure 5b). The seasonal cycle in atmospheric vorticity shows an insignificant difference pre- and post-diversion. From May to August and in December, there is no difference between the long-term monthly mean and monthly mean estimates for pre- and post-diversion (Figure 5b). For other months, the difference does not exceed $\pm 0.7 \text{ s}^{-1}$.

The interannual variability of wind forcing is mainly attributed to year-to-year changes in the cyclonic atmospheric circulation during fall-winter months. The seasonal amplitude of vorticity is significantly diminished in 1953-54, 2001-02 and 2015-2016 when the seasonal mean vorticity index for late fall to the beginning of winter did not exceed 8 s^{-1} (Figure 3a). In contrast, during 1960-65, the vorticity seasonal cycle is amplified with the seasonal mean vorticity index between late



225 fall and early winter up to 28 s^{-1} (Figure 3a). The standard deviation of the monthly mean vorticity shown by error bars in Figure 5b gradually decreases from $\pm 4.5 \text{ s}^{-1}$ in December to $\pm 2.8 \text{ s}^{-1}$ in March-April.

Analysis of the daily vorticity time series sheds light on the origin of seasonality in vorticity. Positive seasonal anomalies from September-December (Figures 3a and 5b) are partly attributed to the occurrence of numerous vorticity peaks. For example, in 1969-70 and 2003-04 (highlighted with yellow shading in Figure 3), the seasonal enhancement of atmospheric vorticity (Figure 6, thick pink line) was partially conditioned by synoptic-scale events recorded during October-
230 November 1969 and 2003 (Figure 6, red line). The strongest vorticity peaks were observed on 18 October and 25 November 1969 ($>4 \text{ s}^{-1}$; Figure 6a) and 15 October and 21 November 2003 ($>5 \text{ s}^{-1}$; Figure 6b). The SLP spatial distribution reveals that each of these peaks is attributable to a cyclone passing over Hudson Bay, with the center of low SLP located over the central Hudson Bay on 18 October and 25 November 1969 (Figures 7a and 7b, respectively) and 15 October and 21 November 2003
235 (Figures 7c and 7d, respectively). The horizontal gradients of SLP over western Hudson Bay ranged from $0.020 \text{ hPa km}^{-1}$ (25 November 1969; Figure 7b) to $0.035 \text{ hPa km}^{-1}$ (21 November 2003; Figure 7d). Overall, from 1 September to 31 December, vorticity exceeded 2 s^{-1} nine and 12 times in 1969 and 2003, respectively. In contrast, from 1 January to 30 April 1970 and 2004, vorticity exceeded 2 s^{-1} only four and seven times, respectively (Figure 6). This suggests that the seasonal cycle in atmospheric vorticity is partially governed by the number and strength of cyclones passing over Hudson Bay.

240 4.3 Local river discharge

The time series of Churchill River discharge (Figure 4a) is dominated by (i) the introduction of the flow diversion in 1977 and (ii) the seasonal hydrologic cycle. The mean discharge dropped by about one-third from $1,190 \text{ m}^3 \text{ s}^{-1}$ (1960-1976) to about $400 \text{ m}^3 \text{ s}^{-1}$ following the diversion in 1977. At the same time, the standard deviation of the mean discharge increased from about ± 300 to $\pm 470 \text{ m}^3 \text{ s}^{-1}$ following the diversion (Figure 4a). This is in line with results by *Déry et al.* (2016). The
245 mean annual timing of maximum river discharge during late spring to summer is not significantly disrupted by the diversion (Figure 5c). The magnitude of the monthly mean discharge pre- to post-diversion, however, reduces from about five-fold in March to about two-and-a-half-fold in May-August (Figure 5c). After diversion, the standard deviation of the monthly mean discharge doubles from May to October (Figure 5c). In contrast, from December to April, the standard deviation of the monthly mean was not significantly impacted by the diversion (Figure 5c).

250 4.4 Sea level response to wind forcing and local river discharge

Our data shows that SLA in Churchill, atmospheric vorticity over Hudson Bay, and Churchill River discharge all show variability dominated by the seasonal cycle (Figures 3a, 4a, and 5). In what follows, SLA at Churchill is first compared to the atmospheric vorticity, and then to the Churchill River discharge, with a main focus on the seasonal cycle.

The correlation between the daily vorticity index and SLA from 1950-2019 and 1960-2019 is 0.48 and 0.47, respectively, with insignificant differences between correlations estimated for periods pre- and post-diversion (0.49 and 0.47, respectively; Figure 3b and Table 1). For the ice-free period from June to November, correlations for whole period, and pre-



and post-diversion increase to 0.54, 0.52 and 0.55 (Table 2), respectively, compared to 0.47, 0.49 and 0.47 for the ice-covered period from December to May (Table 3). We test the difference between correlations estimated for the ice-covered and ice-free seasons using the Fisher z-transformation (Fisher, 1921). Statistical assessment shows that the only differences
260 between correlations estimated for whole period and post-diversion are statistically significant at the 99% confidence level.

The relationship between vorticity and SLA changes significantly from one year to another. The mean annual correlations in Figure 3b show these differences ranging from 0.18 in 1982 to 0.69 in 1991. During periods when the sea level seasonal cycle almost disappears (1981-82 and 1987-88), the mean annual correlation drops to about 0.3 and 0.4, respectively (Figure 3b). When the sea level seasonal cycle is diminished (1962-63 and 2016-17), a modest correlation of
265 ~0.5 is estimated (Figure 3b). For time periods enlarged in Figure 6, the annual mean correlation significantly exceeds the long-term mean of 0.47, attaining 0.65 and 0.57 for 1969-70 and 2004-05, respectively (Figure 3b). The direct linkage between vorticity and SLA is evident in Figure 6. During September-November 1969 and 2003, all significant synoptic peaks in SLA are consistent with those in atmospheric vorticity, including storm surges on 18 October and 25 November 1969 (Figure 6a) and on 15 October and 21 November 2003 (Figure 6b).

In contrast to atmospheric vorticity, the correlation between daily SLA and river discharge is significantly smaller.
270 Through the full record from 1960 to 2019, the correlation is 0.22, with an insignificant difference between pre- and post-diversion (0.20 and 0.23, respectively, Figure 4b and Table 1). For the ice-free period from June to November, correlations drop close to or below the level of statistically significant values for the whole and pre-diversion periods (0.08 and 0.03, respectively), and to 0.11 post-diversion (Table 2) compared to 0.21, 0.12 and 0.19 for the ice-covered period from
275 December to May (Table 3). Note that the difference between correlations estimated for the ice-covered and ice-free seasons is statistically significant for only 1960-2019.

Similar to the linkage between vorticity and SLA, the relationship between river discharge and SLA shows significant interannual variability. Correlations computed through the 365-day moving window show negative to positive values ranging from -0.3 to 0.7 with about 15% of estimates below the level of statistical significance (Figure 4b). Among all
280 events when the amplitude of the sea level seasonal cycle was strongly reduced, only 1962-63 and 1981-82 show statistically significant correlation between river discharge and SLA of ~-0.25 (Figure 4b). For events in 1987-88 and 2016-17, correlation is relatively close to or below the level of statistical significance (Figure 4b). The interannual difference in contribution of river discharge to the sea level variability is also evident for 1969-70 and 2004-05. In 1969-70, the annual mean correlation shows relatively modest contributions of river discharge to sea level variability (correlation $R \sim 0.29$; Figure
285 4b) as compared to correlation with atmospheric vorticity ($R \sim 0.65$; Figure 3b). In 2004-05, however, there is no correlation between SLA and river discharge (Figure 4b), and sea level variability is impacted by wind forcing ($R = 0.57$; Figure 3b).

Overall, our results show that the wind forcing impacts the synoptic and seasonal variability of sea level. In what follows, we use the coefficient of determination (R^2 , where R is correlation coefficient in Tables 1-3) to describe the proportion of the variance in sea level that is explained by the wind forcing, river discharge, and the wind forcing and river
290 discharge together. Through the whole annual cycle from 1960 to 2019, wind forcing explains about 22% of sea level



variability, while river discharge contributes only ~5%. Multiple regression analysis shows that on average, both explain ~28% of sea level variability (Table 1).

Our results also reveal the important role of sea-ice cover and river diversion in modifying controls on sea level variability. During the ice-free seasons from 1960-1976, the contribution of wind forcing is 27%, and the role of river discharge is negligible (Table 2). Post-diversion, cyclonic wind forcing and river discharge contribute 30% and 1%, respectively. Together they explain up to 32% of sea level variability (Table 2). During the ice-covered season, the contribution of vorticity is reduced to 22%, with insignificant difference between pre- and post-diversion (Table 3). The contribution of river discharge varies from 1% for pre-diversion to 4% for post-diversion. Wind and river forcing together explain ~27% of sea level variability for both pre- and post-diversion periods (Table 3). Summarizing these results, we point out that the sea-ice cover reduces the influence of wind forcing, and the influence of local river discharge is slightly increased primarily during the ice covered post-diversion period. Post-diversion, the magnitude of river discharge was reduced about three-fold, but seasonal variability increased by a factor of 1.5 (Figure 4a and Déry et al., 2016). Thus, we attribute the increase in river discharge forcing during the post-diversion period mainly to the higher variability in river discharge from May to November (Figure 4a, 5c, and Déry et al., 2016). Note that during May about 85% of Hudson Bay is ice covered (Tivy et al., 2010), and the standard deviation of the monthly mean discharge in May increases from about ± 170 pre-diversion to $\pm 380 \text{ m}^3 \text{ s}^{-1}$ post-diversion.

5 Discussion

Our results show that sea level variability at Churchill is primarily impacted by wind forcing, with discharge from the Churchill River playing a secondary role. Overall, the atmospheric vorticity explains up to 30% of sea level variability at Churchill, with local river discharge contributing up to only 5% (Tables 1-3). This suggests that in western Hudson Bay the northerly winds associated with cyclonic wind forcing (Figure 2b) generate storm surge along the coast due to a surface Ekman on-shore transport. This is consistent with results from Dmitrenko et al. (2020), who used mooring records and Churchill tide gauge observations in 2016-17 to identify this mechanism.

The SLA seasonal cycle in Figure 5a is only partially explained by seasonality in cyclonic wind forcing and local river discharge. The SLA seasonal cycle is also consistent with summertime warming and freshening, and wintertime cooling and salinification. During the ice-free summer period, the water column warms, and seawater becomes less dense and expands, causing the thermosteric sea-level rise. In addition, during summer, riverine water and sea-ice meltwater decrease salinity of the Bay, thus, causing the halosteric sea-level rise. It seems that these factors can explain the residual fraction of the SLA seasonal variability that is not explained by wind forcing and local river discharge. However, the detailed assessment of the thermosteric and halosteric contributions to the Hudson Bay sea level variability is beyond the scope of this paper. In this context, we point out that we examine only the direct impact of the river discharge on the sea level in the Churchill River mouth ignoring the cumulative effect of riverine water on steric height. This simplification



seems to be reasonable because the residence time of the riverine water fraction in southwestern Hudson Bay during summer is ~1-3 months (Granskog et al., 2009).

325 For the seasonal time scales, increased cyclonic activity during fall to early winter impacts the seasonal cycle in SLA. In contrast to Gough and Robinson (2000), we assert that a positive SLA from September-November (Figure 5a) is attributed to enhanced atmospheric vorticity rather than to the local river discharge. The signature of the local river discharge is, however, traceable through the SLA seasonal cycle. During the pre-diversion period, positive SLA in June (Figure 5a) appears to be linked to the spring freshet of the Churchill River (Figures 5a and 5c). However, post-diversion this positive
330 SLA in June vanishes due to the abrupt decrease in the Churchill River discharge during the spring freshet from ~1,500 to 700 m³ s⁻¹ (Figure 5c). Gradual decreases in Churchill River discharge from June/July to April for both pre- and post-diversion cannot explain the positive SLA from fall to winter, especially during the post-diversion period when the mean annual Churchill River discharge decreases to ~400 m³ s⁻¹ (Figure 5c). Note that the cumulative effect of riverine water on steric height is neglected.

335 An additional perspective on SLA response to atmospheric and river forcing comes from a comparison of the monthly mean vorticity and Churchill River discharge time series' with SLA at Churchill for the whole period of river discharge observations, and the pre- and post-diversion periods (Figures 8a, 8b, and 8c, respectively). The SLA patterns for the whole period of river discharge observation (Figure 8a) are strongly impacted by changes in the magnitude of discharge during the pre- and post-diversion periods, as previously discussed. In contrast, the SLA patterns compiled for the pre- and
340 post-diversion periods (Figures 8b and 8c, respectively) provide more precise features of the SLA response to atmospheric and river forcing. In general, comparing atmospheric vorticity to sea level at Churchill shows that cyclones generate positive SLA up to 0.15 m (Figure 8c). The maximum SLA response to cyclonic atmospheric forcing is observed during the ice-free period (pink shading and white circles in Figures 8b and 8c), which is consistent with results of the correlation analysis (Tables 2 and 3). The combination of anticyclonic (negative) vorticity and low river discharge generates negative SLA up to
345 0.09 m during both ice-free and ice-covered seasons (blue shading in Figures 8b and 8c).

The zero SLA contour in Figure 8b and 8c is displaced relative to the zero vorticity and the long-term mean river discharge for the pre- and post-diversion periods. This indicates that these two predictors alone are insufficient to entirely explain the sea level variability, and that there must be other contributing factors. Correlation analysis (Tables 2 and 3) suggests that sea-ice also plays a role in modifying the impact of atmospheric forcing on SLA. In this context, Figures 8
350 reveals the role of sea-ice cover for generating the SLA. The sea level at Churchill exhibits negative SLA while atmospheric vorticity is positive, but not exceeding ~6-8 s⁻¹ (Figure 8). This situation is usually observed during the ice-covered season when river discharge is below the annual mean (blue circles and blue shading in Figures 8b and 8c). We attribute this disruption to the sea-ice cover. Throughout the entire year, positive SLA is generated in response to strong cyclones with vorticity exceeding ~6-8 s⁻¹ regardless of the river discharge contribution and sea-ice conditions (red shading in Figure 8 for
355 vorticity >~6-8 s⁻¹). During the ice-covered season, at relatively low river discharge (<1,200 m³ s⁻¹ and 350 m³ s⁻¹ for pre- and post-diversion, respectively), negative SLA is associated with positive vorticity <6-8 s⁻¹ (blue circles and blue shading in



Figures 8b and 8c). Thus, vorticity $\sim 6\text{-}8\text{ s}^{-1}$ is suggested to be a very rough estimate of the vorticity threshold attributed to the sea-ice impact. Above this threshold, sea-ice does not eliminate wind stress from the water column, and wind forcing impacts sea level variability in Churchill year-round. Below this threshold, sea-ice eliminates wind forcing and a negative
360 SLA is conditioned by low river discharge. When the Churchill River discharge exceeds the monthly means of 1,500-1,600 $\text{m}^3\text{ s}^{-1}$ and $\sim 900\text{ m}^3\text{ s}^{-1}$ for pre- and post-diversion periods, respectively, positive SLA results regardless of wind forcing.

Our results on the mechanisms of sea level variability at Churchill differ from those obtained by Gough and Robinson (2000). First, using sea level and river discharge data from 1974-1994, they found that correlation between Churchill River discharge and SLA in Churchill explains 43% of sea level variability (versus the 5% derived in our analysis).
365 Second, Gough and Robinson (2000) explain a positive SLA observed in Churchill from October-November by the river discharge pulse into the James Bay region with an advective lag of $\sim 4\text{-}5$ months. Furthermore, Gough et al. (2005) speculate that positive SLA during fall is attributed to the James Bay riverine water fraction, which does not exit the Bay through Hudson Strait, but instead re-circulates in western Hudson Bay. The halosteric sea level changes associated with this freshwater fraction are suggested to generate a positive SLA observed in Churchill from October-November. The pathway of
370 this water and the reason for disrupting the mean cyclonic circulation in the Bay were, however, neither specified in Gough and Robinson (2000) nor in Gough et al. (2005). The distance from James Bay to Churchill measured along the coast is roughly 1,000 km. For a 120-150-day lag between peaks in river discharge to James Bay in June (Déry et al., 2005) and maximum positive SLA at Churchill in November, this distance suggests the unrealistic rate of mean advective velocity to be $\sim 8\text{-}10\text{ cm s}^{-1}$. Note that Dmitrenko et al. (2020) estimated the velocity of the northward flow along the western coast of
375 Hudson Bay during strong cyclonic storms to $\sim 13\text{ cm s}^{-1}$, which significantly exceeds the annual mean meridional transport of $\sim 1\text{-}2\text{ cm s}^{-1}$.

Overall, the hypothesis by Gough and Robinson (2000) and Gough et al. (2005) is suggestive of the seasonal disruption of the Hudson Bay cyclonic circulation that is in line with the seasonal pattern of atmospheric vorticity in Figure 5b. Based on satellite altimetry and numerical simulation, Ridenour et al. (2019a) revealed a seasonal reversal to anticyclonic
380 circulation in southwestern Hudson Bay from May-July, with a return to strong cyclonic circulation in fall in response to the seasonal patterns of surface stress. This is consistent with the seasonal cycles of vorticity presented in Figure 5b. However, among $\sim 120\text{-}150$ days of the hypothetical transit time from James Bay to Churchill, the anticyclonic atmospheric forcing is persistently observed only during May-July; in August, vorticity returns to cyclonic (Figure 5b). In the three months before the occurrence of the positive SLA at Churchill in November, the atmospheric forcing has already returned to cyclonic
385 (Figure 5b). In this context, the hypothesis by Gough and Robinson (2000) and Gough et al. (2005) seems to be inconsistent. In what follows, we provide additional arguments to support our finding on the role of wind forcing in generating the SLA at Churchill.

First, Tushingam (1992) provide the time series of sea level at Churchill and the Churchill River discharge from 1972 to 1989 (Figure 5 from Tushingam, 1992). These time series' clearly show an overall low positive correlation
390 completely disrupted in 1973-74, 1977, and 1987-86, which is consistent with our analysis (Figure 4). For 1973-74 and



1987-86, the annual-mean correlation was estimated to be about -0.1 and is below the level of statistical significance (Figure 4b). Overall, from 1960 to 2019, there were 19 events that lasted up to 1.8 years in duration when correlations between the SLA and river discharge were statistically insignificant or even negative (Figure 4b). Note that the period from 1972 to 1989 used by Tushingham (1992) overlaps with the majority of the period from 1974 to 1994 used by Gough and Robinson
395 (2000).

Second, Ward et al. (2018) analyzed daily data from the Global Runoff Data Centre for 187 stations including Churchill and daily maxima sea level data from the Global Extreme Sea-level Analysis. They found no statistically significant dependence between annual maxima of the Churchill River discharge and sea level. For comparison, along the Pacific coast of North America, the correlation ranged from 0.2 to 0.4, and accounted for 4-16% of the variation in sea level.
400 Third, our analysis shows that the seasonal cycle in sea level variability with positive SLA during fall is observed not only in Churchill, but also along the eastern coast of Hudson Bay in Innujjuak (Figures 1 and 9). While the sea level record at Innujjuak is short and not continuous, a positive SLA is recognizable during fall 1969-70 and 1973-76 (Figure 9, blue line). Note that the seasonal SLA at Innujjuak cannot be generated locally because the annual mean (1964-2000) discharge of the local Innujjuak River is only $3.3 \text{ km}^3 \text{ year}^{-1}$, about three times smaller than the Churchill River discharge post-diversion
405 (Godin et al., 2017). In contrast, the seasonal pattern in SLA at Innujjuak is generated by the same cyclonic forcing as in Churchill. Seasonal SLA in Innujjuak is consistent with seasonal amplification of atmospheric vorticity (Figures 5b and 9). Moreover, in Innujjuak, the sea level peaks on 18 October and 25 November 1969 are coherent with peaks in atmospheric vorticity (Figure 9) and sea level at Churchill (Figure 6a). From the preceding analysis we explicitly know that these two vorticity peaks were generated by cyclones passing over the Bay (Figure 7a). The coherent peaks in sea level in Churchill
410 and Innujjuak suggest that cyclones that were centered over Hudson Bay on 18 October and 25 November 1969 generated storm surge on both the eastern and western coasts of Hudson Bay. This is also supported by a coherent response of sea level to atmospheric forcing at Cape Jones Island and North Kopak Island (Figures 1 and 9). Our hypothesis is also consistent with results of sea level numerical simulations in response to cyclones passing over the Bay in 2016-17 (Dmitrenko et al., 2020). For synoptic storm surges, on-shore Ekman transport increases the mass of water column along the coast (the barotropic
415 component). The seasonal baroclinic component appears during summer when water is fresher and warmer causing the thermosteric and halosteric sea-level rise along the coast.

Fourth, satellite altimetry reveals a spatially uniform response of sea level to the seasonal cycle in atmospheric vorticity along the whole coast of Hudson Bay (Figure 10). For 1993-2020, we examine the difference between the sea surface heights (SSH) during summer, when monthly mean atmospheric vorticity changes from -0.7 s^{-1} in June to 1.1 s^{-1} in
420 August, and fall, when vorticity increases from 4.2 s^{-1} in September to 7.3 s^{-1} in November (Figure 5b). Results suggest that enhanced cyclonic vorticity during fall generates seasonal SSH elevation over the entire coast of Hudson Bay with SSH differences between fall and summer ranging from $>5 \text{ cm}$ in James Bay to $\sim 1 \text{ cm}$ along the northwest coast (Figure 10). This confirms our results that a positive SLA during fall is generated over the entire coast of Hudson Bay, and particularly in Churchill and Innujjuak, in response to enhanced cyclonic wind forcing (Figures 5a, 5b, and 9).



425 One may suggest that seasonal SSH elevation in Figure 10 can be partly due to the thermosteric and halosteric sea-level rise. During summer, the Hudson Bay coastal domain receives large amount of fresh and warm water from river runoff. The seasonal tendency for river discharge, however, is opposite to that for the SSH in Figure 10. For 1988-2000, Déry et al. (2005) reported that the total discharge of rivers flowing into Hudson Bay peaks in June at $\sim 3.6 \text{ km}^3 \text{ day}^{-1}$, which significantly exceeds the secondary maximum in October ($\sim 2.3 \text{ km}^3 \text{ day}^{-1}$). The seasonal mean total river discharge in
430 September-November ($\sim 1.9 \text{ km}^3 \text{ day}^{-1}$) is one-and-a-half times smaller compared to $\sim 2.8 \text{ km}^3 \text{ day}^{-1}$ in June-August. Based on these estimates, the river discharge seasonal cycle in June-November is inconsistent with that for the SSH in Figure 10. The cumulative effect of river discharge on the seasonal cycle can play a role, but the residence time of the riverine water fraction in southwestern Hudson Bay during summer is relatively small (~ 1 -3 months; Granskog et al., 2009).

Finally, our results on the atmospheric forcing of the Hudson Bay SLA are in agreement with conclusions by
435 Piecuch and Ponte (2014, 2015). Using ocean mass measurements from satellite gravimetry conducted during the Gravity Recovery and Climate Experiment, they found that wind forcing dominates sea-level and mass variability in Hudson Bay, and wind might drive Hudson Bay mass changes due to wind-driven outflow through Hudson Strait (Piecuch and Ponte; 2014). For the sea level interannual variability in Hudson Bay, also evident in Figure 4a, Piecuch and Ponte (2015) revealed a wind-driven barotropic fluctuation that explains most of the non-seasonal sea level variance. Furthermore, they suggest that
440 anomalous inflow and outflow through Hudson Strait, which impacts sea level variability in Hudson Bay, are driven by wind stress over Hudson Strait. This highlights the role of wind forcing in amplifying the freshwater outflow from Hudson Bay, as also suggested by Straneo and Saucier (2008) and Dmitrenko et al. (2020).

In summary, we suggest that seasonal amplification of atmospheric vorticity, partially conditioned by the number and strength of cyclones passing over the Bay during fall to early winter, generates the seasonal cycle in sea level variability
445 over the entire Bay as depicted schematically in Figure 11. Cyclones passing over Hudson Bay during fall to early winter cause on-shore Ekman transport and storm surges over the entire coast of Hudson Bay (Figure 11a). In summer, anticyclonic wind forces off-shore Ekman transport lowering sea level along the coastline of Hudson Bay (Figure 11b).

6 Summary and conclusions

Our analysis revealed that in contrast to previous research, the local Churchill River discharge explains only up to 5% of the
450 sea level variability at Churchill. While, cyclonic atmospheric forcing is shown to explain from 22% during the ice-covered winter-spring season to 30% during the ice-free summer-fall season (Tables 1-3). Multiple regression analysis showed that atmospheric forcing and local river discharge together can explain up to 32% of the sea level variability at Churchill. We found that a positive sea level anomaly in Churchill during fall is partially conditioned by the seasonal cycle in atmospheric vorticity, with prevailing cyclonic wind forcing during fall to the beginning of winter (Figure 5). Sea-ice cover reduces wind
455 stress on the water column during the ice-covered season from December to May, and cyclonic wind forcing generates positive sea level anomalies at Churchill when only the monthly mean vorticity exceeds ~ 6 -8 s^{-1} (Figure 8).



We expanded our observations at Churchill to the bay-wide scale using sea level observations along the eastern coast of the Bay and satellite altimetry. A coherent sea level response to atmospheric forcing observed at the opposite sides of Hudson Bay suggests that the spatial scale of cyclones passing over Hudson Bay roughly equals the Hudson Bay area (Figures 7 and 9, and *Dmitrenko et al.*, 2020). This scaling equivalency implies that cyclones passing over Hudson Bay cause on-shore Ekman transport and storm surges over the entire Hudson Bay coast (Figure 11a). This is also consistent with results by *Dmitrenko et al.* (2020) obtained for 2016-17. Moreover, the satellite altimetry data shows that this scaling equivalency works not only for synoptic, but also for the seasonal time scale. The seasonal cycle in atmospheric vorticity (Figure 5b) partially conditions the seasonal cycle in sea level variability over the entire coast of Hudson Bay. The recurring cyclonic wind forcing during fall favors sea level elevation over the entire Hudson Bay coast compared to summer (Figures 10 and 11). This seasonal pattern in sea level variability has an important implication for geostrophic circulation. The cross-shelf pressure gradient generated due to seasonal amplification of sea level along the coast drives alongshore geostrophic flow and favors the cyclonic circulation around Hudson Bay during fall to earlier winter. In contrast, during summer the geostrophic component attributed to the anticyclonic atmospheric forcing disrupts the Hudson Bay cyclonic circulation as shown by *Ridenour et al.* (2019a).

Our research is important for maritime activity within the Bay. Communities around the Bay highly rely on the annual summer sea-lift to re-supply them at a fraction of the price compared to air transport (*Kuzyk and Candlish*, 2019). In this context, positive coastal sea level anomalies during fall favor re-supply operations to coastal communities. However, increased cyclonic activity during fall is also associated with extreme wind events (Figure 2b) and storm surges (e.g., Figure 6) increasing risks to re-supply and fuel-transfer operations.

The origin of seasonality in cyclonic wind forcing, its climatic aspects and ocean response to seasonal and interannual variability in atmospheric vorticity over the Bay are among important priorities for our future research. The freshwater storage in Hudson Bay and export through Hudson Strait seem to be directly impacted by seasonal and interannual variability in wind forcing, clearly defining the need for further research in this area using multi-year numerical simulations and atmospheric reanalyses. Seasonality of the wind forcing is the hypothesized cause of the sea level variability, but probably does not provide a complete explanation. The steric changes in coastal zone attributed to river runoff were not taken into account that points out a necessity for future research involving numerical simulations.

Acknowledgments

This work is a part of research conducted under the framework of the Arctic Science Partnership (ASP) and ArcticNet. This research is also a contribution to the Natural Sciences and Engineering Council of Canada (NSERC) Collaborative Research and Development project: BaySys (CRDPJ470028-14). Funding for this work was provided by NSERC, Manitoba Hydro, the Canada Excellence Research Chair (CERC) program, the Canada Research Chairs (CRC) program and the Canada-150 Research Chairs program. D. Babb is additionally supported by NSERC and the Canadian Meteorological and



Oceanographic Society (CMOS). DLV was supported under the auspices of the Cooperative Institute for Marine and
490 Atmospheric Studies (CIMAS), a cooperative institute of the University of Miami and NOAA, cooperative agreement
NA20OAR4320472.

Data

The sea level data are available through <http://www.isdm-gdsi.gc.ca/isdm-gdsi/twl-mne/index-eng.htm#s5>.

Authors' contributions

495 Conceptualization: ID
Methodology: ID, DV, TS, AT
Formal analysis: ID, DV, AT
Investigation: ID, DV, AC, TS
Resources: KS, DBarber
500 Data curation: ID, DV, AT
Writing (original draft): ID, DV, TS
Writing (review & editing): AC, DV, SK, TS, AT, DBabb
Visualization: ID, DV
Supervision: DBarber
505 Project administration: KS, DBarber
Funding acquisition: KS, DBarber.
Approved the submitted version for publication: ID

Competing interests

The authors declared no competing interests.

510 References

Andrews, J., Babb, D., and Barber, D.G., Climate change and sea ice: Shipping accessibility on the marine transportation
corridor through Hudson Bay and Hudson Strait (1980–2014), *Elem. Sci. Anth.*, 5, 15, doi: 10.1525/elementa.13, 2017.
Copernicus Climate Change Service (C3S), ERA5: Fifth generation of ECMWF atmospheric reanalyses of the global
climate. Copernicus Climate Change Service Climate Data Store (CDS). Available at
515 <https://cds.climate.copernicus.eu/cdsapp#!/home>, 2017.



- Déry, S. J., Stieglitz, M., McKenna, E.C., and Wood, E.F., Characteristics and trends of river discharge into Hudson, James, and Ungava Bays, 1964–2000, *J. Climate*, 18, 2540–2557, doi: 10.1175/JCLI3440.1, 2005.
- Déry, S.J., Mlynowski, T.J., Hernández-Henríquez, M.A., and Straneo, F., Interannual Variability and Interdecadal Trends in Hudson Bay Streamflow, *Journal of Marine Systems*, 88(3), 341–351, doi: 10.1016/j.jmarsys.2010.12.002, 2011.
- 520 Déry, S.J., Stadnyk, T.A., MacDonald, M.K., and Gauli-Sharma, B., Recent trends and variability in river discharge across northern Canada, *Hydrology and Earth System Sciences*, 20(12), doi: 10.5194/hess-20-4801-2016, 2016.
- Dmitrenko, I.A., Kirillov, S.A., and Tremblay, L.B., The long-term and interannual variability of summer fresh water storage over the eastern Siberian shelf: Implication for climatic change, *J. Geophys. Res.*, 113, C03007, doi: 10.1029/2007JC004304, 2008a.
- 525 Dmitrenko, I.A., Kirillov, S.A., Tremblay, L.B., Bauch, D., and Makhotin, M., Effects of atmospheric vorticity on the seasonal hydrographic cycle over the eastern Siberian shelf, *Geophys. Res. Lett.*, 35, L03619, doi: 10.1029/2007GL032739, 2008b.
- Dmitrenko, I.A., Myers, P.G., Kirillov, S.A., Babb, D.G., Volkov, D.L., Lukovich, J.V., Tao, R., Ehn, J.K., Sydor, K., and Barber, D.G., Atmospheric vorticity sets the basin-scale circulation in Hudson Bay, *Elem. Sci. Anth.*, 8, 49, doi: 530 10.1525/elementa.049, 2020.
- Dmitrenko, I.A., Kirillov, S.A., Babb, D.G., Kuzyk, Z.A., Basu, A., Ehn, J.K., Sydor, K., and Barber, D.G., Storm-driven hydrography of western Hudson Bay, submitted to *Continental Shelf Res.*, 2021.
- Eastwood, R.A., McDonald, R., Ehn, J., Heath, J., Arragutainaq, L., Myers, P.G., Barber, D., and Kuzyk, Z.A., Role of river runoff and sea-ice brine rejection in controlling stratification throughout winter in southeast Hudson Bay, *Estuaries and* 535 *Coasts*, doi: 10.1007/s12237-020-00698-0, 2020.
- Fisher, R.A., On the 'probable error' of a coefficient of correlation deduced from a small sample, *Metron*, 1, 3–32, 1921.
- Godin, P., Macdonald, R.W., Kuzyk, Z.Z.A., Goñi, M.A., and Stern, G.A., Organic matter compositions of rivers draining into Hudson Bay: Present-day trends and potential as recorders of future climate change, *J. Geophys. Res. Biogeosci.*, 122, 1848–1869, doi: 10.1002/2016JG003569, 2017.
- 540 Gough, W.A., Projections of sea-level change in Hudson and James Bays, Canada, due to global warming, *Arctic and Alpine Research*, 30(1), 84–88, doi: 10.2307/1551748. 1998.
- Gough, W.A., and Robinson, C.A., Sea-level Variation in Hudson Bay, Canada, from Tide-Gauge Data, *Arctic, Antarctic, and Alpine Research*, 32(3), 331–335, doi: 10.1080/15230430.2000.12003371, 2000.
- Gough, W.A., Robinson, C., and Hosseinian, R., The Influence of James Bay River Discharge on Churchill, Manitoba Sea 545 Level, *Polar Geography*, 29(5), 213–223, doi: 10.1080/789610202, 2005.
- Granskog, M.A., Macdonald, R.W., Kuzyk, Z.A., Senneville, S., Mundy, C.-J., Barber, D.G., Stern, G.A., and Saucier, F., Coastal conduit in southwestern Hudson Bay (Canada) in summer: Rapid transit of freshwater and significant loss of colored dissolved organic matter, *J. Geophys. Res.*, 114, C08012, doi: 10.1029/2009JC005270, 2009.



- Granskog, M.A., Kuzyk, Z.A., Azetsu-Scott, K., and Macdonald, R.W., Distributions of runoff, sea-ice melt and brine using
550 $\delta^{18}\text{O}$ and salinity data - A new view on freshwater cycling in Hudson Bay, *Journal of Marine Systems*, 88, 362–374, doi:
10.1016/j.jmarsys.2011.03.011, 2011.
- Guttenberg, B., Changes in sea level, postglacial uplift, and mobility of the earth's interior, *Geological Society of America
Bulletin*, 52(5), 721–772, doi: 10.1130/GSAB-52-721, 1941.
- Hersbach, H., and Coauthors, The ERA5 global reanalysis, *Quarterly Journal of the Royal Meteorological Society*, 146,
555 1999–2049, doi: 10.1002/qj.3803, 2020.
- Hochheim, K.P., and Barber, D.G., Atmospheric forcing of sea ice in Hudson Bay during the fall period, 1980–2005, *J.
Geophys. Res.*, 115, C05009, doi: 10.1029/2009JC005334, 2010.
- Hochheim, K.P., and Barber, D.G., An update on the ice climatology of the Hudson Bay System, *Arctic Antarctic Alpine
Res.*, 46(1), 66–83, doi: 10.1657/1938-4246-46.1.66, 2014.
- 560 Ingram, R.G., and Prinsenberg, S., Coastal oceanography of Hudson Bay and surrounding Eastern Canadian Arctic Waters,
In: Robinson, A.R., and Brink, K.N. (Eds.), *The Sea*, Vol. 11. *The Global Coastal Ocean Regional Studies and Synthesis*.
Harvard University Press, Cambridge, Massachusetts and London, 835–861, 1998
- Kalnay, E., Kanamitsu, M., Kistler, R., Collins, W., Deaven, D., Gandin, L., Iredell, M., Saha, S., White, G., Woollen, J.,
Zhu, Y., Chelliah, M., Ebisuzaki, W., Higgins, W., Janowiak, J., Mo, K. C., Ropelewski, C., Wang, J., Leetmaa, A.,
565 Reynolds, R., Jenne, R., and Joseph, D., The NCEP/NCAR 40-year reanalysis project, *Bull. Am. Meteorol. Soc.*, 77, 437–
471, doi: 10.1175/1520-0477(1996)077<0437: TNYRP>2.0.CO;2, 1996.
- Kuzyk, Z.A., Macdonald, R.W., Stern, G.A., and Gobeil, C., Inferences about the modern organic carbon cycle from
diagenesis of redox-sensitive elements in Hudson Bay, *Journal of Marine Systems*, 88, 451–462, doi:
10.1016/j.jmarsys.2010.11.001, 2011.
- 570 Kuzyk, Z.A., and Candlish, L.M., *From Science to Policy in the Greater Hudson Bay Marine Region: An Integrated
Regional Impact Study (IRIS) of Climate Change and Modernization*, ArcticNet, Québec City, 424 pp., 2019.
- Landy, J.C., Ehn, J.K., Babb, D.G., Theriault, N., and Barber, D.G., Sea ice thickness in the eastern Canadian Arctic:
Hudson Bay complex & Baffin Bay, *Remote Sensing of Environment*, 200, 281–294, doi: 10.1016/j.rse.2017.08.019, 2017.
- Larson, K.M., and van Dam, T., Measuring postglacial rebound with GPS and absolute gravity, *Geophys. Res. Lett.*, 27,
575 3925–3928, doi: 10.1029/2000GL011946, 2000.
- Mulet, S., Rio, M.H., Greiner, E., Picot, N., and Pascual, A., New global Mean Dynamic Topography from a GOCE geoid
model, altimeter measurements and oceanographic in-situ data, OSTST Boulder, USA, available at:
http://www.aviso.altimetry.fr/fileadmin/documents/OSTST/2013/oral/mulet_MDT_CNES_CLS13.pdf, 2013.
- Piecuch, C.G., and Ponte, R.M., A wind-driven nonseasonal barotropic fluctuation of the Canadian inland seas, *Ocean Sci.*,
580 11, 175–185, doi: 10.5194/os-11-175-2015, 2015.
- Piecuch, C.G., and Ponte, R.M., Nonseasonal mass fluctuations in the midlatitude North Atlantic Ocean, *Geophys. Res.
Lett.*, 41, 4261–4269, doi: 10.1002/2014GL060248, 2014.



- Prinsenbergh, S.J., Freshwater contents and heat budgets of James Bay and Hudson Bay, *Continental Shelf Res.*, 3(2), 191-200, doi: 10.1016/0278-4343(84)90007-4, 1984.
- 585 Prinsenbergh, S.J., Salinity and temperature distribution of Hudson Bay and James Bay, In: Martini, E. P. (ed.) *Canadian Inland Seas*, Oceanogr. Ser. 44, Elsevier, New York, 163–186, 1986a.
- Prinsenbergh, S.J., The circulation pattern and current structure of Hudson. In: Martini, E. P. (ed.) *Canadian Inland Seas*, Oceanogr. Ser. 44, Elsevier, New York, 187–203, 1986b.
- Prinsenbergh, S.J., Ice-cover and ice-ridge contributions to the freshwater contents of Hudson Bay and Foxe Basin, Arctic, 590 41(1), 6–11, doi: 10.14430/arctic1686, 1988.
- Prinsenbergh, S.J., Effects of hydro-electric projects on Hudson Bay's marine and ice environments, *Potential Environ. Impacts Ser. 2*, 8 pp., North Wind Inf. Serv., Montreal, 1991.
- Pujol, M.-I., Faugère, Y., Taburet, G., Dupuy, S., Pelloquin, C., Ablain, M., and Picot, N., DUACS DT2014: the new multi-mission altimeter data set reprocessed over 20 years, *Ocean Sci.*, 12, 1067-1090, doi: 0.5194/os-12-1067-2016, 2016.
- 595 Pew Charitable Trusts, *The Integrated Arctic Corridors Framework. Planning for responsible shipping in Canada's Arctic waters*, available at: <https://www.pewtrusts.org/~media/Assets/2016/04/The-Integrated-Arctic-Corridors-Framework.pdf>, 2016.
- Ray, R.D., Sea Level, Land Motion, and the Anomalous Tide at Churchill, Hudson Bay, American Geophysical Union, Fall Meeting 2015, abstract id. G43B-1040, 2015.
- 600 Ridenour, N.A., Hu, X., Sydor, K., Myers, P.G., and Barber, D.G., Revisiting the circulation of Hudson Bay: Evidence for a seasonal pattern, *Geophysical Research Letters*, 46, 3891–3899, doi: 10.1029/2019GL082344, 2019a.
- Ridenour, N.A., Hu, X., Jafarikhazragh, S., Landy, J.C., Lukovich, J.V., Stadnyk, T.A., Sydor, K., Myers, P.G., and Barber, D.G., Sensitivity of freshwater dynamics to ocean model resolution and river discharge forcing in the Hudson Bay Complex, *Journal of Marine Systems*, 196, 48-64, doi: 10.1016/j.jmarsys.2019.04.002, 2019b.
- 605 Sella, G.F., Stein, S., Dixon, T.H., Craymer, M., James, T.S., Mazzotti, S., and Dokka, R.K., Observation of glacial isostatic adjustment in “stable” North America with GPS, *Geophys. Res. Lett.*, 34, L02306, doi: 10.1029/2006GL027081, 2007.
- Smith, C.A., Compo, G.P., and Hooper, D.K., Web-based reanalysis intercomparison tools (WRIT) for analysis and comparison of reanalyses and other datasets, *Bull. Amer. Meteor. Soc.*, 95(11), 1671–1678, doi: 10.1175/BAMS-D-13-00192.1, 2014.
- 610 Saucier, F.J., and Dionne, J., A 3-D coupled ice-ocean model applied to Hudson Bay, Canada: The seasonal cycle and time-dependent climate response to atmospheric forcing and runoff, *J. Geophys. Res. Oceans*, 103(C12), 27,689-27,705, doi: 10.1029/98JC02066, 1998.
- Saucier, F.J., Senneville, S., Prinsenbergh, S., Roy, F., Smith, G., Gachon, P., Caya, D., and Laprise, R., Modelling the sea ice-ocean seasonal cycle in Hudson Bay, Foxe Basin and Hudson Strait, Canada, *Climate Dynamics*, 23, 303–326, doi: 615 10.1007/s00382-004-0445-6, 2004.



- St-Laurent, P., Straneo, F., Dumais, J.-F., and Barber, D.G., What is the fate of the river waters of Hudson Bay?, *Journal of Marine Systems*, 88, 352–361, doi: 10.1016/j.jmarsys.2011.02.004, 2011.
- Straneo, F., and Saucier, F., The outflow from Hudson Strait and its contribution to the Labrador Current, *Deep-Sea Res. I*, 55, 926–946, doi: 10.1016/j.dsr.2008.03.012, 2008.
- 620 Tivy, A., Howell, S.E., Alt, B., Yackel, J.J., and Carrieres, T., Origins and levels of seasonal forecast skill for sea ice in Hudson Bay using Canonical Correlation Analysis, *J. Climate*, 24(5), 1378-1395, doi: 10.1175/2010JCLI3527.1, 2011.
- Tushingham, A.M., Observations of postglacial uplift at Churchill, Manitoba, *Canadian Journal of Earth Sciences*, 29, 2418-2425, doi: 10.1139/e92-189, 1992.
- Ward, P.J., Couasnon, A., Eilander, D., Haigh, I.D., Hendry, A., Muis, S., Veldkamp, T.I.E., Winsemius, H.C., and Wahl, T.,
 625 Dependence between high sea-level and high river discharge increases flood hazard in global deltas and estuaries, *Environ. Res. Lett.*, 13, 084012, doi: 10.1088/1748-9326/aad400, 2018.
- Walsh, J.E., Chapman, W.L., and Shy, T.L., Recent decrease of sea level pressure in the central Arctic, *J. Climate*, 9, 480–486, doi: 10.1175/1520-0442(1996)009<0480:RDOSLP>2.0.CO;2, 1996.
- Wang, J., Mysak, L.A., and Ingram, R.G., A Three-Dimensional Numerical Simulation of Hudson Bay Summer Ocean
 630 Circulation: Topographic Gyres, Separations, and Coastal Jets, *J. Phys. Oceanogr.*, 24, 2496–2514, doi: 10.1175/1520-0485(1994)024<2496:ATDNSO>2.0.CO;2, 1994.
- Wolf, D., Klemann, V., and Wunsch, J., A Reanalysis and Reinterpretation of Geodetic and Geological Evidence of Glacial-Isostatic Adjustment in the Churchill Region, Hudson Bay, *Surv. Geophys.*, 27, 19–61, doi: 10.1007/s10712-005-0641-x, 2006.

635 **Tables**

Table 1: Correlations (*R*) of daily atmospheric vorticity and/or Churchill River discharge and sea level anomalies in western Hudson Bay for the whole annual cycle

Predictor(s)/Time frame	1960 - 2019	Pre-diversion 1960 - 1976	Post-diversion 1977 - 2019
Vorticity	0.47	0.49	0.47
River discharge	0.22	0.20	0.23
Vorticity and river discharge*	0.53*	0.53*	0.53*



640 **Table 2:** Correlations (R) of monthly-mean atmospheric vorticity and/or Churchill River discharge and sea level anomalies in western Hudson Bay for the ice-free period (June-November)

Predictor(s)/Time frame	1960 - 2019	Pre-diversion 1960 - 1976	Post-diversion 1977 - 2019
Vorticity	0.54	0.52	0.55
River discharge	0.08	0.03**	0.11
Vorticity and river discharge*	0.55*	0.52*	0.57*

Table 3: Correlations (R) of monthly-mean atmospheric vorticity and/or Churchill River discharge and sea level anomalies in western Hudson Bay for the ice-covered period (December-May)

Predictor(s)/Time frame	1960 - 2019	Pre-diversion 1960 - 1976	Post-diversion 1977 - 2019
Vorticity	0.47	0.49	0.47
River discharge	0.21	0.12	0.19
Vorticity and river discharge*	0.52*	0.51*	0.52*

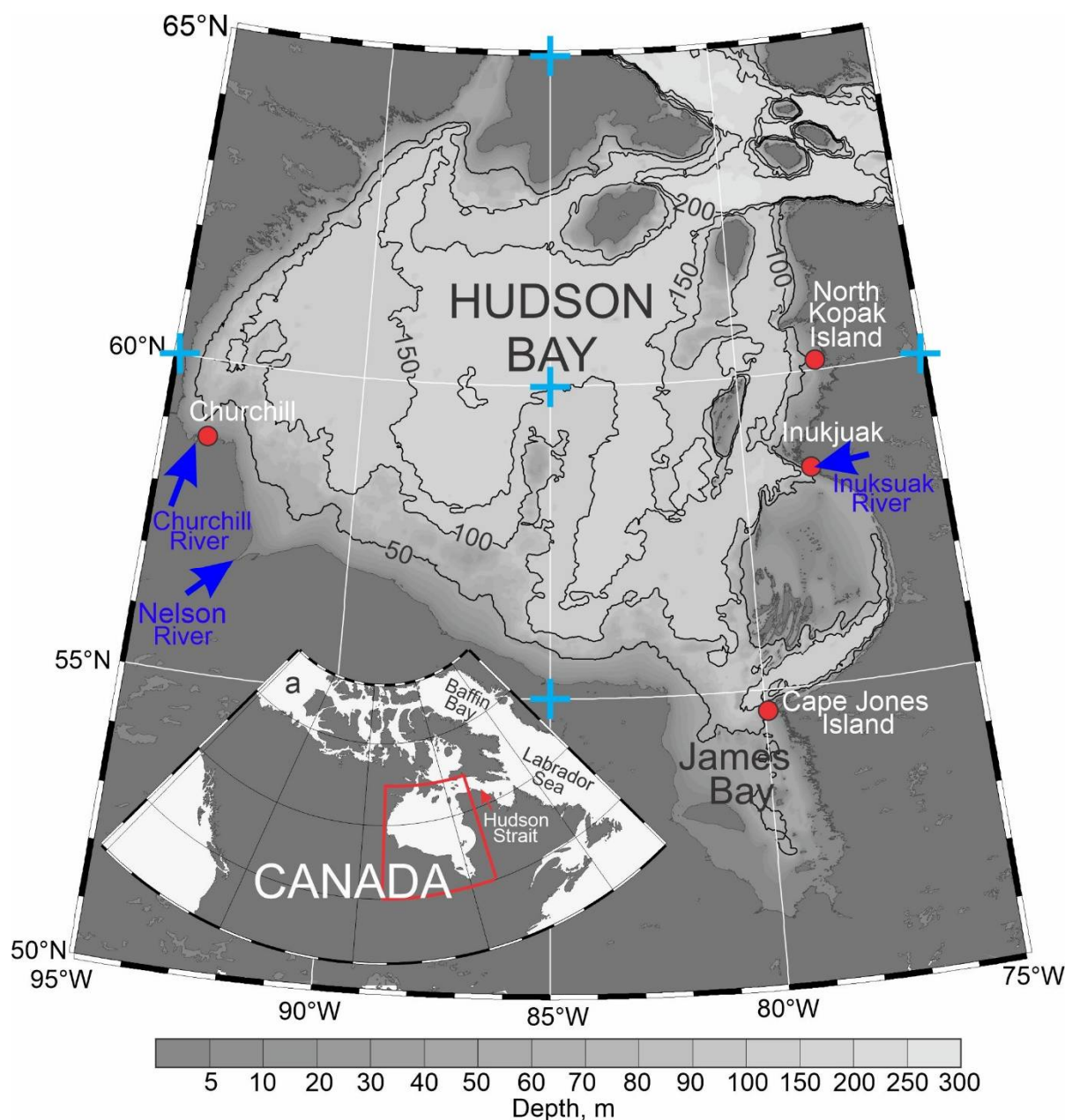
645

*The coefficient of multiple correlation is estimated based on the multiple linear regression analysis

** Correlation not statistically significant at the 99% confidence level



Figures



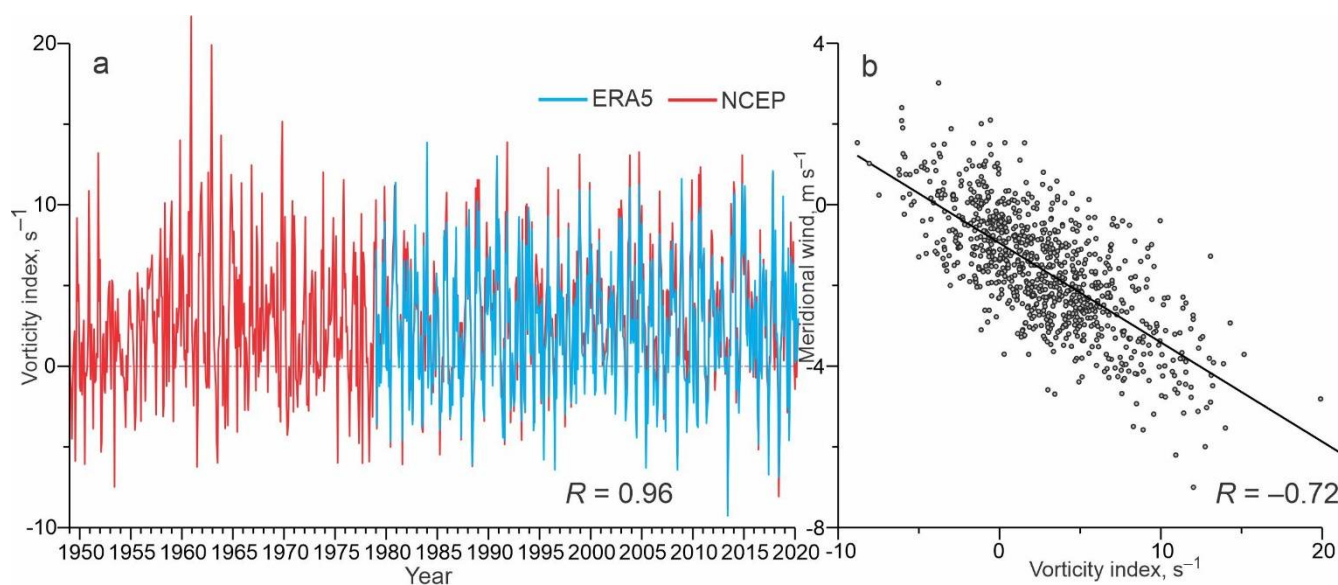
650

Figure 1: Map of Hudson Bay. Red dots depict the permanent tide gauge in Churchill and temporary tide gauges in Inukjuak, Cape Jones Island and North Kopak Island. Blue arrows highlight Churchill, Nelson and Inuksuak river mouths. Blue crosses depict the 5-point stencil used for computing atmospheric vorticity approximated as Laplacian from sea level atmospheric pressure. The numbered black lines depict depth contours of 50, 100, 150 and 200 m. (a) Inset shows the

655 Hudson Bay location within North America. The map of Hudson Bay was compiled based on the General Bathymetric Chart of the Oceans (GEBCO, www.gebco.net).



660



665

Figure 2: (a) Time series of the monthly mean atmospheric vorticity index (s^{-1}) over Hudson Bay, derived from NCEP (red) and ERA5 (blue). (b) Scatter plot of the monthly mean meridional wind seaward of Churchill in western Hudson Bay ($m s^{-1}$) versus the monthly mean atmospheric vorticity index. Thick black line depicts linear regression. Numbers at the bottom show correlation R between (a) the monthly mean vorticity derived from NCEP and ERA5 (1970-2000) and (b) the monthly mean vorticity and meridional wind (1949-2020).

670

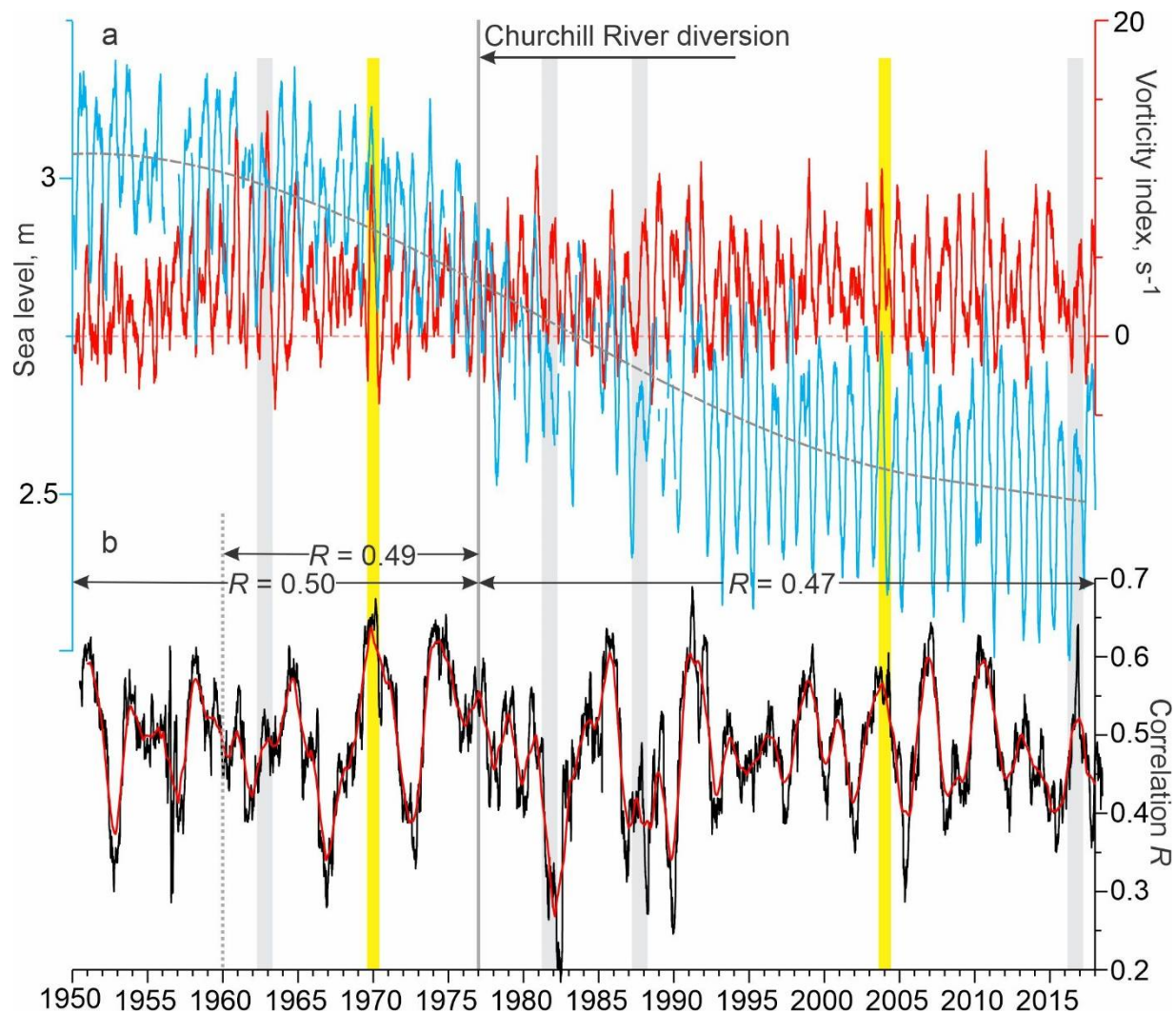
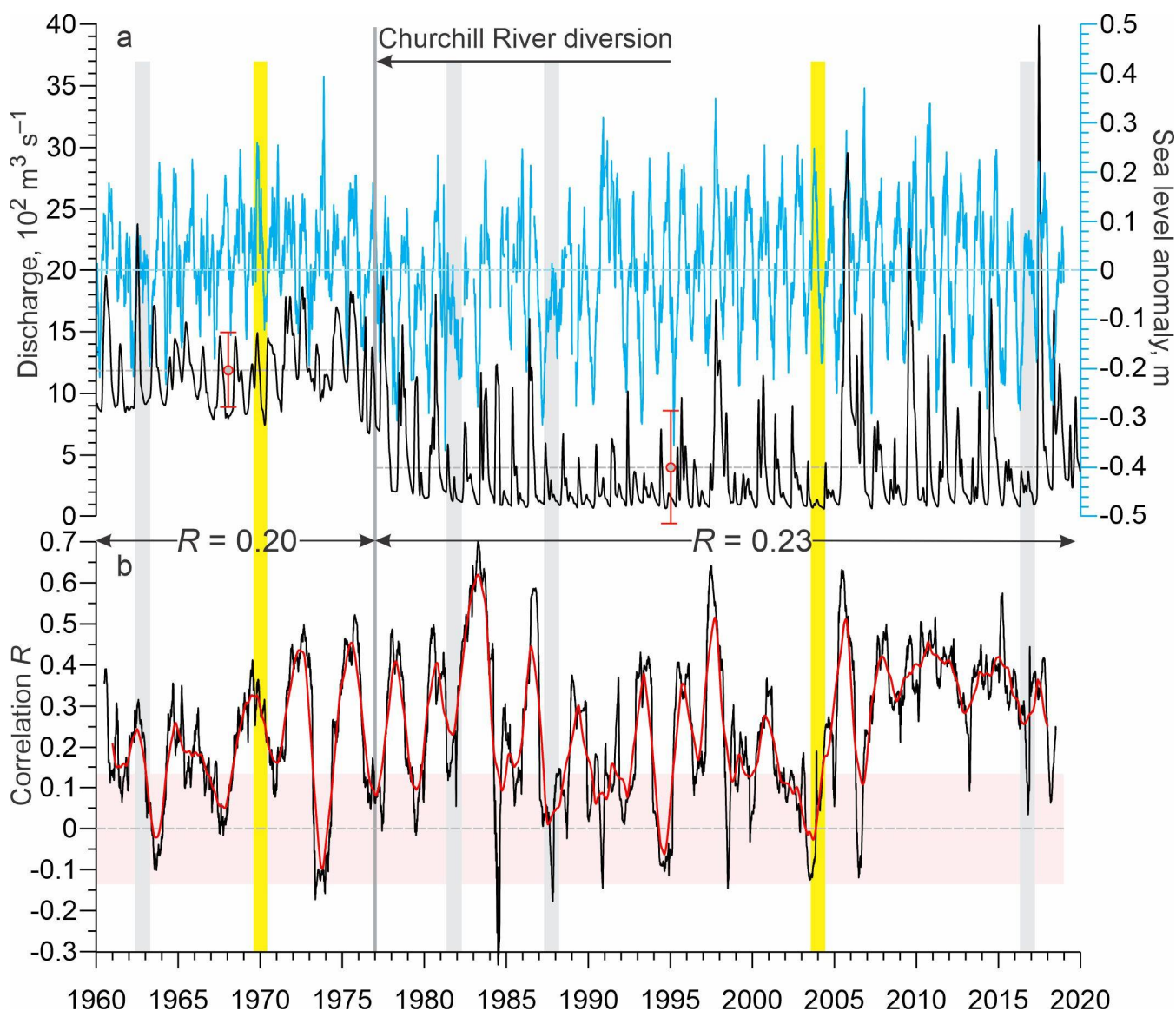


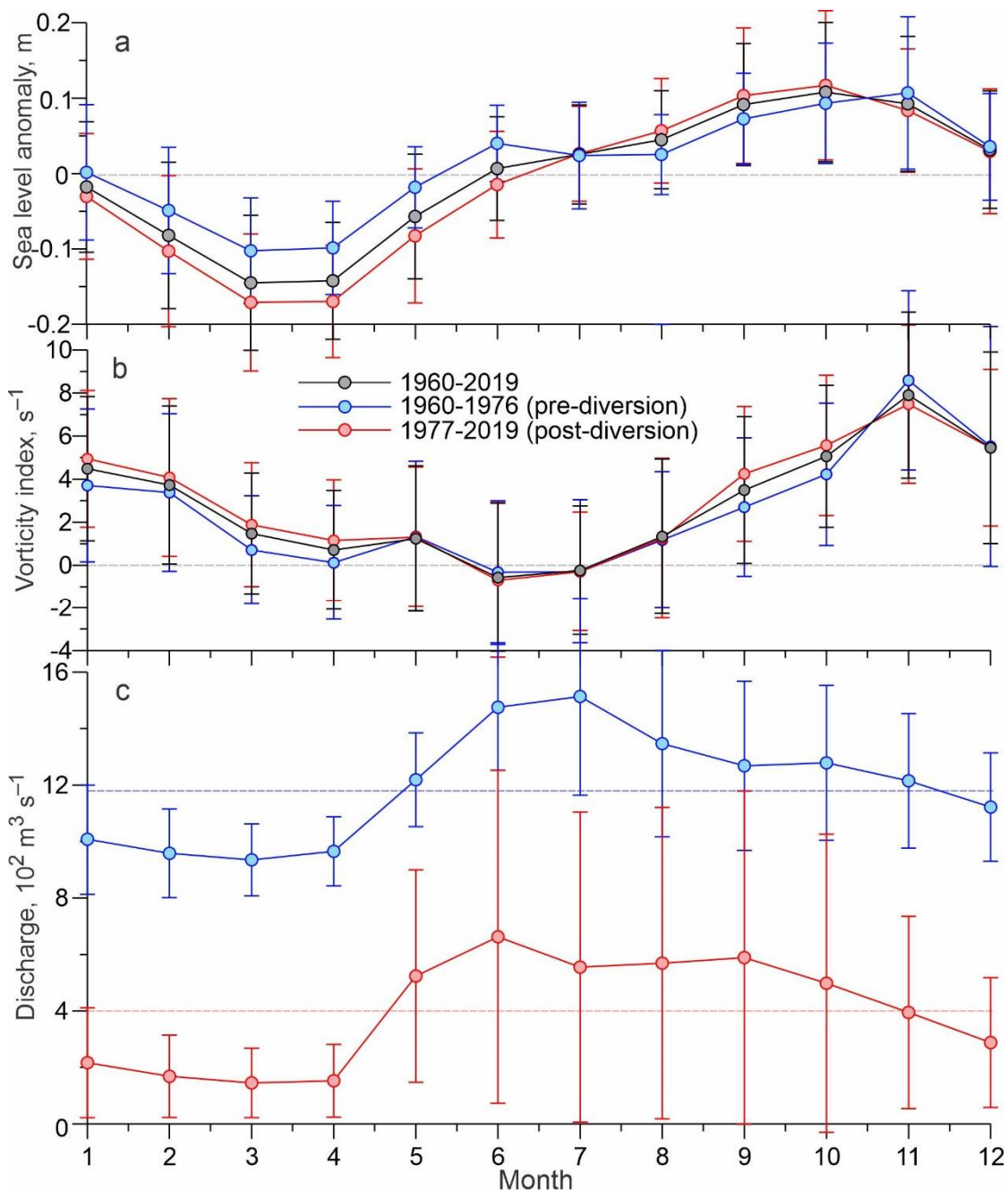
Figure 3: (a) 91-day running mean of daily atmospheric vorticity index (red, s^{-1}) over Hudson Bay and daily mean sea level
 675 measured at the tide gauge in Churchill (blue, m). Positive and negative vorticity correspond to cyclonic and anticyclonic
 atmospheric circulation, respectively. Gray dashed line shows polynomial approximation of the sea level trend attributed to
 the glacial isostatic adjustment. (b) Correlation R between daily vorticity index and sea level anomaly (SLA) computed for
 the 365-day moving window (black) with their 365-day running mean (red). All correlations are statistically significant at
 99% confidence. Numbers at the top show correlation between daily vorticity index and SLA computed for 1950/60-1976
 680 and 1977-2018 pre- and post-diversion, respectively. (a, b) Yellow shading highlights August-May 1969-70 and 2003-04,
 enlarged in Figure 6. Black arrow indicates onset of the Churchill River diversion. Gray shading highlights periods when the
 sea level seasonal cycle was partially disrupted (1981-82 and 1987-88), or significantly diminished (1962-63 and 2016-
 2017).



685

690

Figure 4: (a) 30-day running mean of the Churchill River discharge (black; $10^2 \text{ m}^3 \text{ s}^{-1}$) and detrended daily mean SLA at Churchill (blue; m). Gray circles show mean discharge pre- and post-diversion with standard deviations depicted with red error bars. (b) Correlation R between daily Churchill River discharge and SLA computed for the 365-day moving window (black) with their 365-day running mean (red). Pink shading highlights statistically insignificant correlations at the 99% confidence level. Numbers at the top show correlation between daily Churchill River discharge and SLA computed for 1950-1976 and 1977-2018 pre- and post-diversion, respectively. (a, b) Yellow shading highlights August-May 1969-70 and 2003-04. Black arrow indicates onset of the Churchill River diversion. Gray shading highlights periods when the sea level seasonal cycle was partially disrupted (1981-82 and 1987-88), or significantly diminished (1962-63 and 2016-2017).



695

Figure 5: Seasonal cycle of (a) SLA at Churchill (m), (b) atmospheric vorticity over Hudson Bay (s^{-1}), and (c) Churchill River discharge ($10^2 m^3 s^{-1}$). Seasonal cycle derived using monthly-mean data for (a, b) 1950-2019 (black), (a, b) 1950-76 (blue) and (c) 1960-76 (blue) before the Churchill River diversion, and (a, b, c) 1977-2018 (red) after the Churchill River diversion. Error bars show \pm one standard deviation of the mean. (c) Blue and pink dashed lines show the long-term mean discharge before and after diversion, respectively.

700

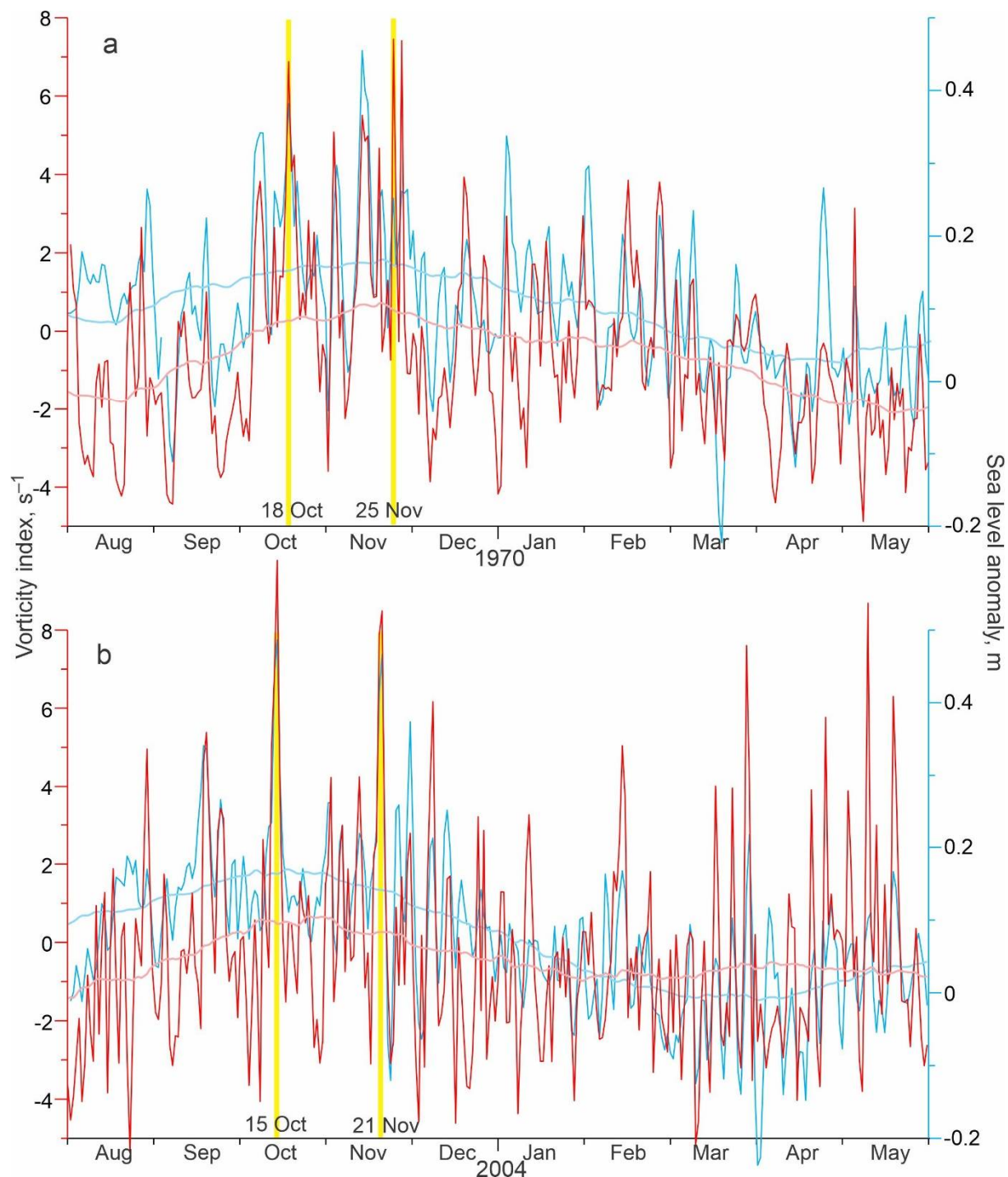


Figure 6: Time series of the daily mean vorticity index (red; s⁻¹) and SLA at Churchill (blue; m) with their 91-day running mean in pink and light blue, respectively, for August/May (a) 1969/1970 and (b) 2003/2004. (a, b) Vertical yellow lines highlight coherent peaks in vorticity and sea level in October and November.



705

710

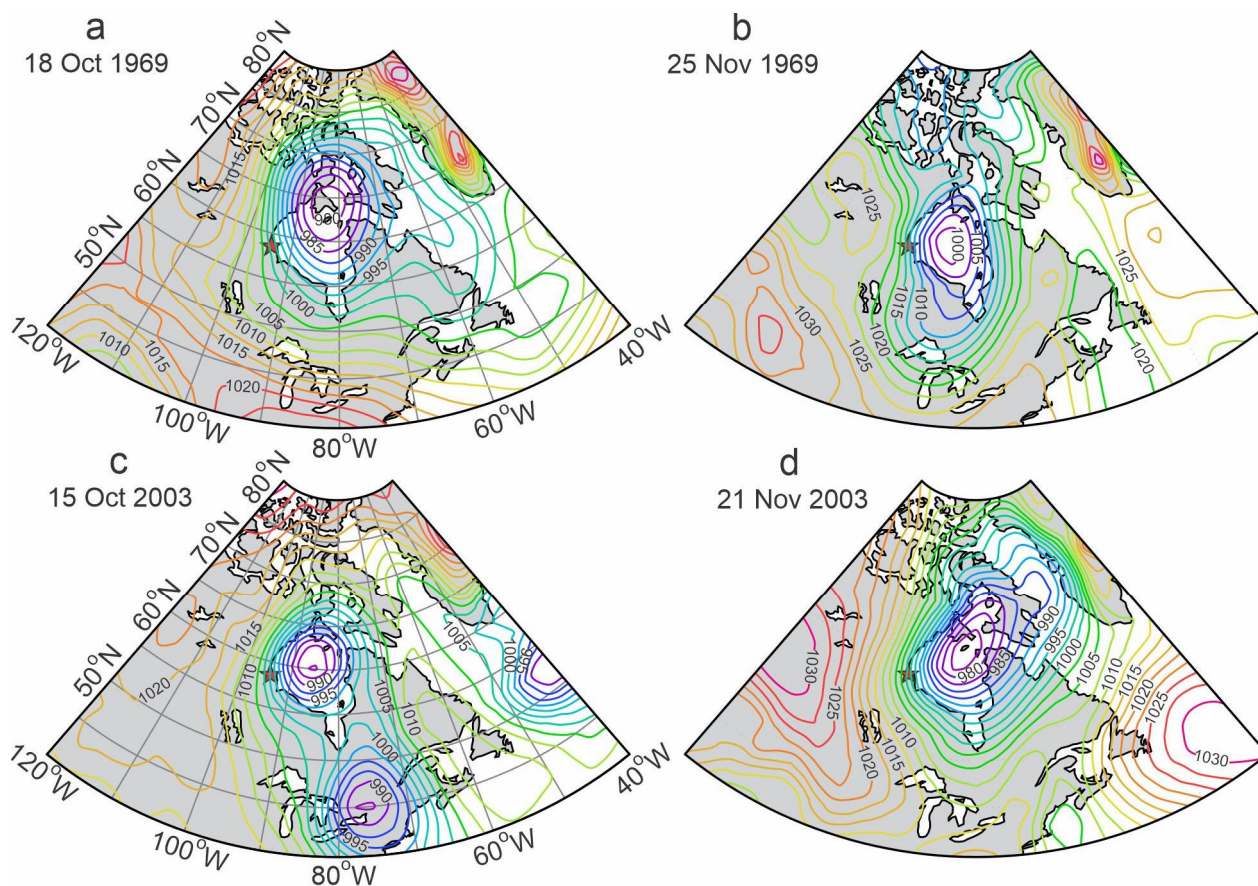
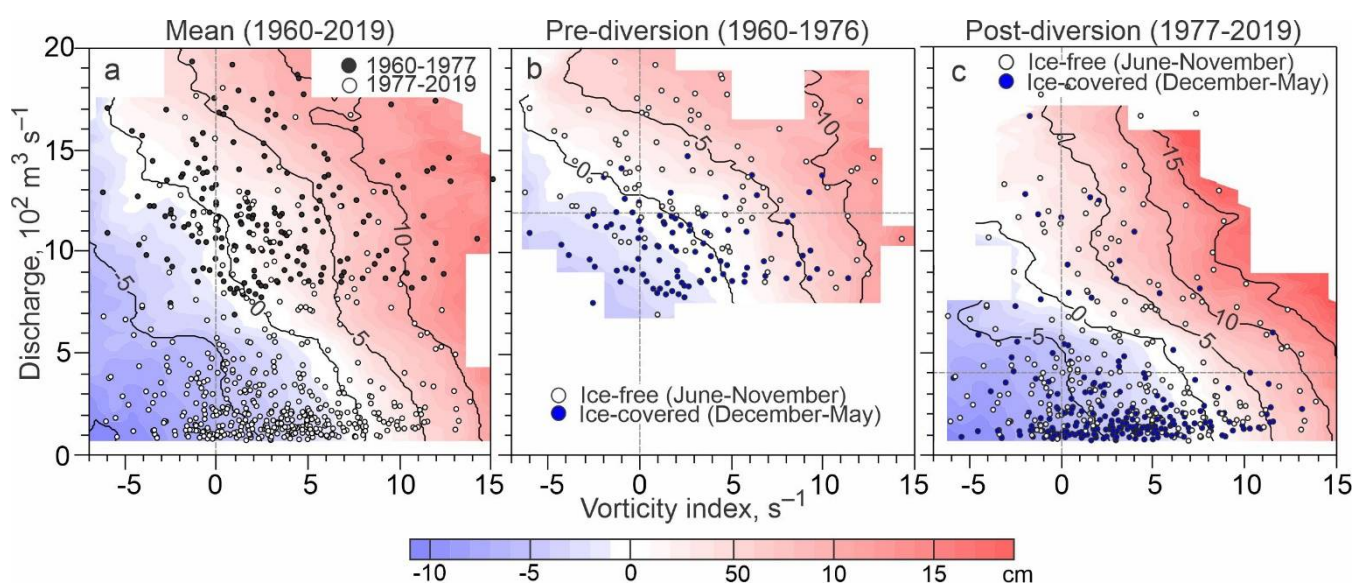


Figure 7: Sea level atmospheric pressure (hPa) for coherent peaks in atmospheric vorticity and sea level at Churchill, highlighted in Figure 6 with yellow lines: (a) 18 October 1969, (b) 25 November 1969, (c) 15 October 2003, and (d) 21 November 2003.

715



720



725

Figure 8: Color shading shows monthly mean sea level anomalies (cm) from tidal gauge at Churchill versus atmospheric vorticity (s^{-1} ; horizontal axis) and Churchill River discharge ($10^2 m^3 s^{-1}$; vertical axis) for (a) entire period of river discharge observations (1960 – 2019), and (b) before and (c) after the Churchill River diversion in 1977. Scatter plots show monthly mean vorticity and river discharge for (a) 1960-1976 (black circles) and 1977-2019 (white circles), and (b, c) ice-free season (June-November; white circles) and ice-covered season (December-May; blue circles). Horizontal gray dashed line shows mean river discharge (c) before and (d) after diversion.

730



735

740

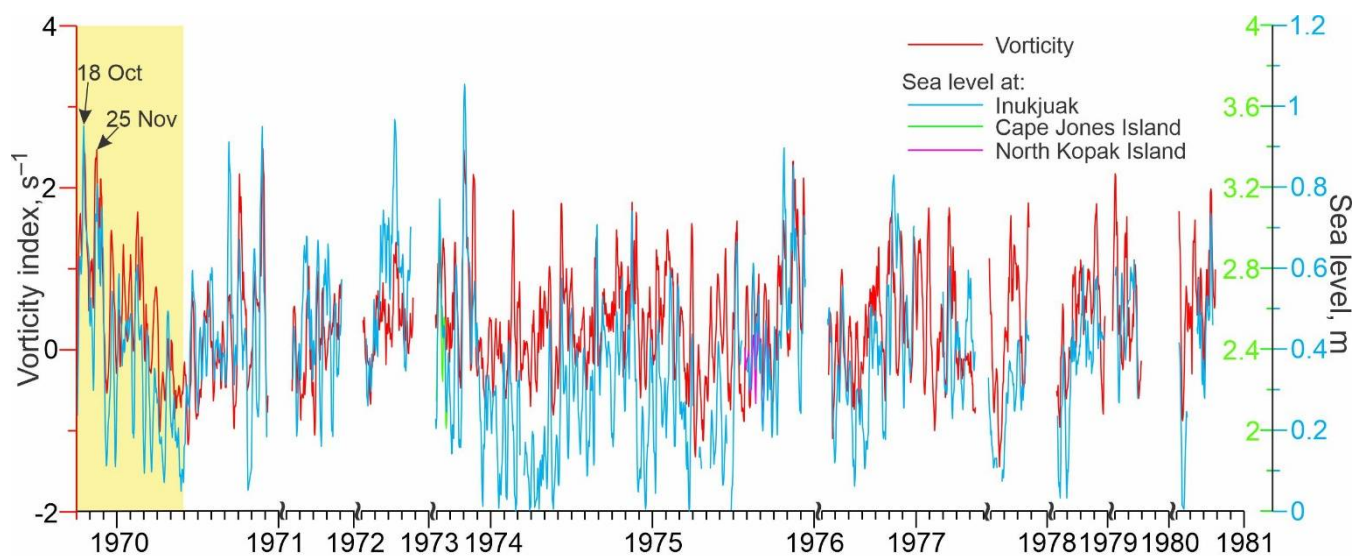
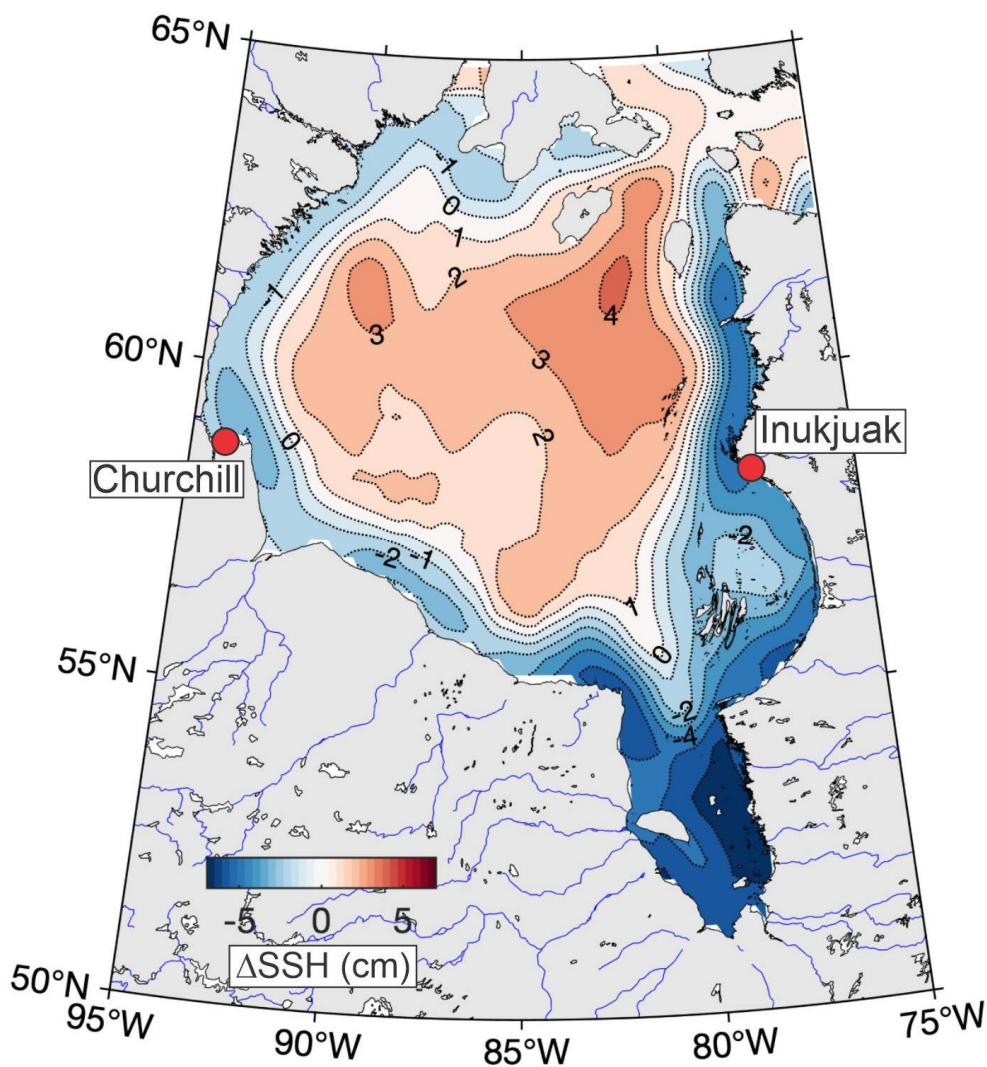


Figure 9: Time series of 7-day running mean for daily atmospheric vorticity index (red, s^{-1}) over Hudson Bay and daily mean sea level (m) measured at the tide gauge in Innukjuak (blue), Cape Jones Island (green) and North Kopak Island (purple). Yellow shading highlights October/May 1969/70. Black arrows indicate two cyclonic storms in 18 October and 25 November 1969 with atmospheric forcing shown in Figures 7a and 7b, respectively. Right vertical axis shows sea-level scale for Innukjuak (blue), and Cape Jones Island and North Kopak Island (green).



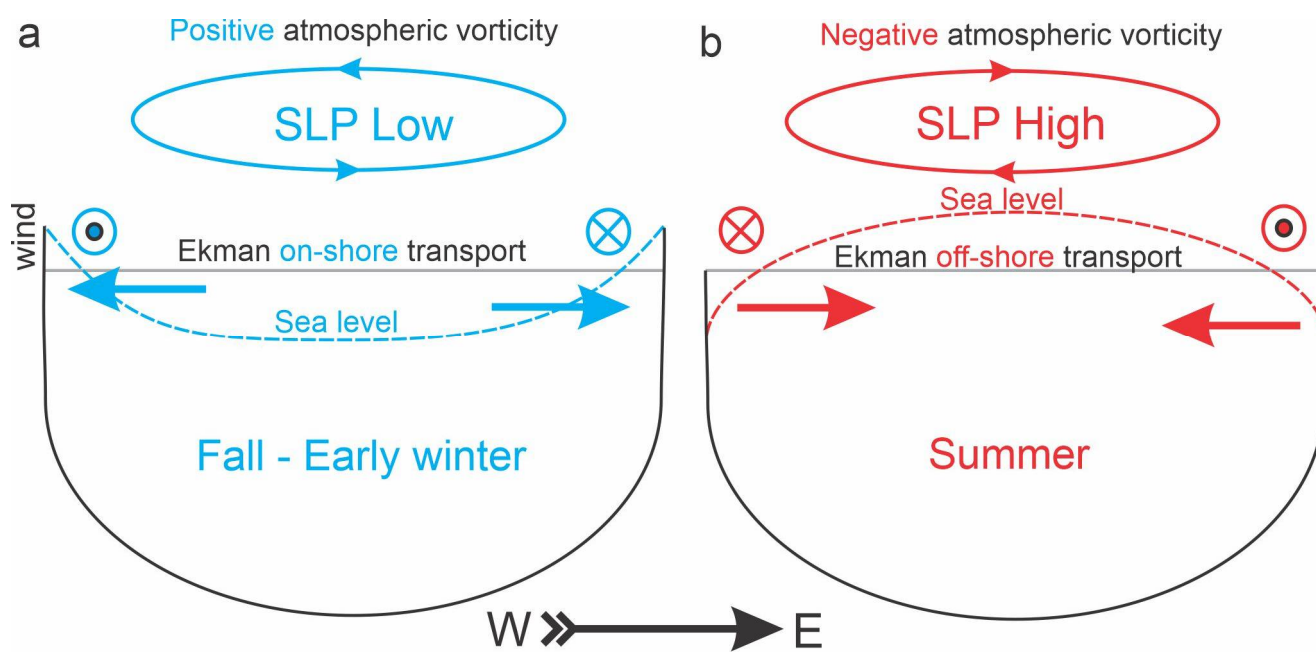
750



755 **Figure 10:** The long-term mean (1993-2020) difference between sea surface height (SSH; cm) in summer (June-August) and fall (September-November) derived from the satellite altimetry. Red dots depict the tide gauge in Churchill and Innukjuak.



760



765

Figure 11: Diagram of the proposed impact of the seasonal changes in atmospheric vorticity on the sea level seasonal variability in Hudson Bay. (a) Positive (cyclonic) vorticity during October-December causes onshore Ekman transport and storm surges over the coast. (b) Negative (anticyclonic) vorticity during June-July forces offshore Ekman transport. During winter, a complete sea-ice cover reduces momentum transfer from wind stress to the water column diminishing impact of atmospheric forcing on sea level variability.

770